

Use Authorization

In presenting this thesis in partial fulfillment of the requirements for an advanced degree at Idaho State University, I agree that the Library shall make it freely available for inspection. I further state that permission to download and/or print my thesis for scholarly purposes may be granted by the Dean of the Graduate School, Dean of my academic division, or by the University Librarian. It is understood that any copying or publication of this thesis for financial gain shall not be allowed without my written permission.

Signature _____

Date _____

DETERMINING THE EFFECTIVENESS
OF A BONNER SPHERE EXTENSION
FOR LOW-ENERGY NEUTRONS

by
Daniel Isaacs

A thesis
submitted in partial fulfillment
of the requirements for the degree of
Master of Science in the Department of Nuclear Engineering
Idaho State University
Spring 2016

To the Graduate Faculty:

The members of the committee appointed to examine the thesis of DANIEL ISAACS find it satisfactory and recommend that it be accepted.

Dr. Eric Burgett,
Major Advisor

Dr. Christopher McGrath,
Committee Member

Dr. David Beard,
Graduate Faculty Representative

For Pailey

TABLE OF CONTENTS

LIST OF FIGURES	vi
LIST OF TABLES	ix
LIST OF EQUATIONS	x
LIST OF ABBREVIATIONS	xi
ABSTRACT	xii
CHAPTER 1: Introduction	1
Background	1
Bonner Sphere Spectroscopy	2
Bonner Sphere Extension	7
CHAPTER 2: Theory	10
Neutron Unfolding	10
CHAPTER 3: Experiment	14
Physical Setup	14
Detector Setup	17
Pelletron Setup	20
Data Analysis	24
CHAPTER 4: Results	38
CHAPTER 5: Conclusions	54
Future Work	55
REFERENCES	56
APPENDIX	58
Unfolding Output Files	58
Additional Plots of the Neutron Spectrum	60
Percent Difference Plots	63
Sphere Properties	65
Detector Measurement Data	67

LIST OF FIGURES

Figure 1: Schematic of neutron interactions in moderated detectors (Knoll, 2000)	3
Figure 2: Response functions of Bonner spheres. Notice the changes in shape and peak location (Johnson, 1987)	5
Figure 3: Evidence of gamma discrimination (Bramblett, 1960)	6
Figure 4: Schematic of neutron interactions in the BSE. The dark outer ring is the high Z-materials, with a thermal neutron detector at the center (Burgett, 2008)	8
Figure 5: Cross section of the large and small assemblies	9
Figure 6: Excerpt from shielding diagram for Pelletron	15
Figure 7: Physical Setup of detector in relation to target and ^{241}Am -Be source	16
Figure 8: Schematic of detector internals and dimensions (Cruzate, 2007)	16
Figure 9: HDPE Bonner spheres	16
Figure 10: BSE hemispheres: copper (bottom), lead (middle), tungsten (top), HDPE covers (right)	17
Figure 11: Setup of electronic modules	19
Figure 12: Picture of electronics and computer interface	19
Figure 13: 4 MV charging schematic for Pelletron (NEC, 2005).	21
Figure 14: Copper Target Schematic a.) front view b.) side view	21
Figure 15: ^{65}Cu (p,n) cross section.	23
Figure 16: MAXED output (.plo) showing chi-squared limit is too low	30
Figure 17: Plotted spectrum for over-iterated chi-squared	30
Figure 18: MAXED output (.plo) showing an acceptable value of chi-squared	31

Figure 19: Plotted spectrum for a normally iterated chi-squared	31
Figure 20: Comparison between .plo and .flu data plots	32
Figure 21: $D r^2$ as a function of r^2 with corresponding trend lines	37
Figure 22: Plot of Count/mC for each BSS measurement distance.	38
Figure 23: Plot of all the unfolded BSS measurements	39
Figure 24: Unfolded neutron spectra for all 3" BSE spheres at the 1 meter location	40
Figure 25: Unfolded neutron spectra for all 5" BSE spheres at the 1 meter location	41
Figure 26: Unfolded spectra for all 3" BSE spheres at the 2 meter location	42
Figure 27: Unfolded spectra for all 5" BSE spheres at the 2 meter location	43
Figure 28: Unfolded spectra for all 3" BSE spheres at the 3 meter location	44
Figure 29: Unfolded spectra for all 5" BSE spheres at the 3 meter location	45
Figure 30: Percent difference in 3" BSE .v. BSS spectra at 1 meter location	46
Figure 31: Percent difference in energy bins of 5" BSE and BSS spectra at 1 meter location	47
Figure 32: 1 meter integral values per bin for BSS and BSE	48
Figure 33: 2 meter integral values per bin for BSS and BSE	49
Figure 34: 3 meter integral values per bin for BSS and BSE	49
Figure 35: Effect of air in-scatter on D_0 and σ_r	52
Figure 36: Plot of measured $^{241}\text{Am-Be}$ spectra against ISO 8529 standard	53
Figure 37: Comparison of 3" copper spheres	60
Figure 38: Comparison of 5" copper spheres	60
Figure 39: Comparison of 3" lead spheres	61

Figure 40: Comparison of 5" lead spheres	61
Figure 41: Comparison of 3" tungsten spheres	62
Figure 42: Comparison of 5" tungsten spheres	62
Figure 43: Percent difference in energy bins of 3" spheres at 3 meters	63
Figure 44: Percent difference in energy bins of 5" spheres at 2 meters	63
Figure 45: Percent difference in energy bins of 3" spheres at 3 meters	64
Figure 46: Percent difference in energy bins of 5" spheres at 3 meters	64

LIST OF TABLES

Table 1: Advantages and disadvantages of BSS (Thomas, 2002)	5
Table 2: Nomenclature of BSE assemblies	7
Table 3: .ibu file for MAXED. Column 3 and 4 are the detector counts and uncertainty, respectively	26
Table 4: Control file (.inp) for MAXED. Column 1 are the parameters and Column 2 explain each parameter	27
Table 5: 1 meter integral value data with comparison	50
Table 6: 2 meter integral value data with comparison	51
Table 7: 3 meter integral value data with comparison	51
Table 8: Negligible effect of air in-scatter on total detector response (D_t) and response to source (D_o)	52
Table 9: Example .flu output from MAXED	58
Table 10: Example of .par output from MAXED	59
Table 11: Physical dimensions of the BSE hemispheres and BSS spheres	65
Table 12: Calculated densities of spheres with percent error	66
Table 13: 1 meter Pelletron detector data	67
Table 14: 2 meter Pelletron detector data	68
Table 15: 3 meter Pelletron detector data	69
Table 16: 4 meter Pelletron detector data	70
Table 17: ^{241}Am -Be detector data	70

LIST OF EQUATIONS

Equation 1: First order Fredholm integral equation	10
Equation 2: Expression for maximizing the entropy	11
Equation 3: Summation notation of the Fredholm integral in Equation 1	12
Equation 4: Constraint for handling ϵ_k	12
Equation 5: Constraint on admissible solutions	12
Equation 6: Expression for solution spectrum in terms of $\{\lambda_k, \gamma\}$	12
Equation 7: Solution for ϵ_k in terms of $\{\lambda_k, \gamma\}$	12
Equation 8: The relationship between coulombs and amperes	25
Equation 9: Total response for room-return correction	35
Equation 10: Simplified equation for determining D_o	35
Equation 11: Equation for fractional room-return correction	35

LIST OF ABBREVIATIONS

BSS	Bonner Sphere Spectrometer
BSE	Bonner Sphere Extension
²⁴¹ Am-Be	Americium-Beryllium neutron source
⁶ LiI (Eu)	lithium-6 iodide scintillator doped with europium
HDPE	high-density polyethylene
MeV	mega electronvolt (1×10^6 eV)
Cu	Copper
Pb	Lead
W	Tungsten
ID	inside diameter
OD	outside diameter
MAXED	Maximum Entropy Deconvolution program
UMG	Unfolding with MAXED and GRAVEL
PMT	photomultiplier tube
Preamp	preamplifier
MCA	multichannel analyzer
NEC	National Electrostatics Corporation
MV	million volts
mrem/hr	millirem per hour
mC	millicoulomb
IAEA	International Atomic Energy Agency
PTB	Physikalisch-Technische Bundesanstalt
ISO	International Organization of Standardization

ABSTRACT

A Bonner Sphere Spectrometer (BSS) was used to measure the neutron spectrum produced by bombarding a copper target with protons accelerated by the RISE 4 MV Tandem Pelletron. The measurement used a commercially-available detector in conjunction with a Bonner Sphere Extension (BSE) developed and tested previously. The resulting neutron spectrum provides important information about the neutron field strength and distribution at different distances from the target for a future experiment utilizing the Pelletron. The unfolded neutron spectrum was used to calculate the integral fluence rates for slow, intermediate, and fast neutron energy bins. The BSE measurements at low energies are uncommon and were compared to the standard BSS data to determine the effectiveness of such a measurement. Despite being designed for use at higher energies, it is shown that certain heavy moderators provide insight into lower energy neutron fields.

The same BSS system was used to measure the neutron spectrum from a ^{241}Am -Be neutron source. The spectrum was compared to existing data from other facilities in order to determine the accuracy of our BSS system. These comparisons also resulted in a preliminary evaluation of the air in-scatter and room-return neutrons and their contribution to the measured spectra. This work provides the basis for developing a calibration factor for the BSS/BSE combination for future measurements using the RISE Pelletron.

CHAPTER 1: Introduction

Background

To ensure the safety of people working around radioactive materials, it is important to know how much radiation is present. Radiation detectors provide this knowledge. Some detectors allow integrated real-time measurement of radiation field strength, while other types can very accurately determine the radiation energies and intensities present (Knoll).

There are three main types of radiation detectors: gas-filled, scintillation, and semiconductor diode. The common gas-filled detectors are: ion chambers used for beta and gamma detection, proportional counters used for low-level gamma or x-ray radiation as well as alpha, beta, in specially designed systems—neutron detection, and Geiger-Müller counters used to count the number of radiation events. Scintillation detectors can be used to measure gamma rays, x-rays, other particles and neutrons but most have poor energy resolution. Semiconductor-diode detectors, on the other hand, provide very good energy resolution of charged particles (Knoll).

Neutron detection is difficult because neutrons carry no charge and can travel several centimeters in matter to meters in air with no interaction. For these reasons, neutron detection relies on nuclear reactions that result in energetic charged particles. Most neutron detectors are designed with a target material to foster the reaction that creates the energetic charged particles in conjunction with one of the detection

methods discussed. Neutron detectors are generally divided into two categories based on the neutron's energy, slow and fast (Knoll).

The detection of slow neutrons (<0.5 eV) contains no information about initial kinetic energy because it is lost in the many collisions required to slow the neutrons. As the neutron energy increases past the resonant region (1-300 eV) into the intermediate (300 eV-0.5 MeV) and fast regions (>0.5 MeV), the initial energy is no longer negligible when compared to the reaction Q-value (the amount of energy released or required by the reaction) so the initial neutron energy can be deduced. If energy is released, then that reaction has a positive Q-value while requiring additional energy for a reaction means that reaction has a negative Q-value

Some applications of fast neutron detection do not require knowledge of the neutron energy, only the ability to measure the presence of neutrons. These types of detectors can use any of the neutron interaction principles used by slow neutron detectors that result in a charged particle emission. However, the detectors will have varying efficiencies based on the incident neutron energy, but will provide information about the relative fast-neutron fluence rate (Knoll).

Bonner Sphere Spectroscopy

Bonner Sphere Spectroscopy is a neutron detection technique developed by Bramblett, Ewing, and Bonner, and utilizes the neutron interaction with a lithium-6 iodide scintillator doped with europium (${}^6\text{LiI}(\text{Eu})$) (Bramblett, 1960). The Eu^{2+} is used as a luminescent activator to create the lattice defects that emit light. The choice of

activator determines the wavelength and decay time of the light when scintillation occurs. ${}^6\text{LiI}$ scintillators are more sensitive to thermal neutrons, so faster neutrons are moderated into the thermal region, but moderation removes any information about the initial kinetic energy of the neutrons. BSS uses different size spheres of high-density polyethylene (HDPE) as neutron moderators. A neutron of unknown initial energy passes through the moderating material until it interacts with the hydrogen in the HDPE. This interaction causes neutron recoil and results in a loss of energy. This interaction can happen several times until the neutron escapes, is absorbed or is detected as shown in Figure 1.

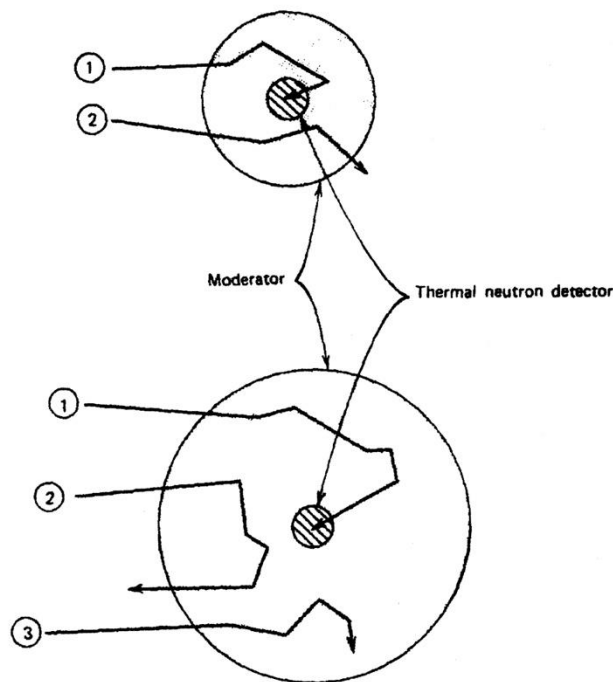


Figure 1: Schematic of neutron interactions in moderated detectors (Knoll, 2000)

As incident neutron energy increases, more neutron moderation is needed in order to slow the neutrons into a detectable energy range for the scintillator. However, as the moderator increases in size, it decreases the probability of a neutron interacting

with the scintillator and increases the probability of neutron absorption in the moderator because the increased number of interactions results in lower neutron energies. For this reason moderating spheres of different sizes are carefully selected such that the overall efficiency curve matches the requirements for specific applications (Knoll).

The size of each moderator corresponds to a specific region of the measured neutron spectrum where that moderator has the greatest probability of resulting in a detectable neutron. The probability curve for each sphere is called a response curve. The detector outputs can be used in a deconvolution method to determine the initial neutron energies from the source because of the associated response functions. Each response curve has a slightly different peak location and overlaps with neighboring curves (Figure 2), allowing the entire set of moderators to be used to build a single neutron spectrum from the data collected (Knoll).

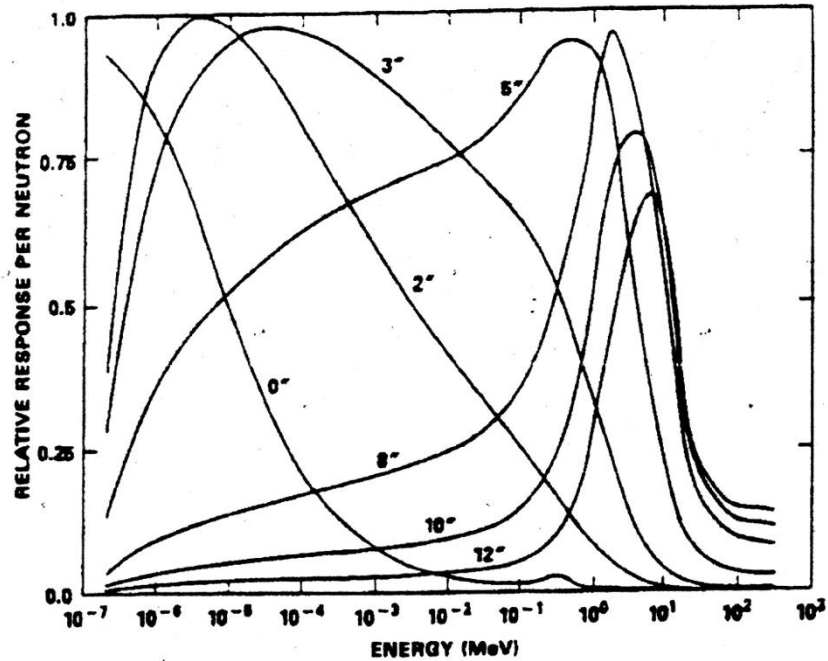


Figure 2: Response functions of Bonner spheres. Notice the changes in shape and peak location (Johnson, 1987)

Bonner Spheres were selected for this experiment, despite their disadvantages (Table 1), for their versatility across a broad range of energies present in accelerator facilities and for their isotropic response.

Characteristic	Verdict	Comment
Energy Resolution	Poor	Restricted by similarity of response functions available
Energy Range	Excellent	The only spectrometer presently available which will cover the energy range from thermal to the GeV region
Sensitivity	Good	High Sensitivity by comparison with other neutron spectrometers, and can be varied by changing the thermal sensor
Operation	Simple but lengthy	Making measurements is simple, with no really complex electronics, but it can be time consuming
Angular Response	Isotropic	Do not need to know the direction of the neutron field. Ideal for deriving ambient dose equivalent, but provides no angular data for deriving effective dose
Spectrum Unfolding	Potential for errors	Complex unfolding code required, and the under-determined problem means that any solution is not unique; significant errors are possible
Photon Discrimination	Good	By the choice of an appropriate sensor systems can be made insensitive, even to intense photon fields

Table 1: Advantages and disadvantages of BSS (Thomas, 2002)

The ${}^6\text{LiI}$ scintillator is placed at the center of six HDPE spheres ranging from 2-12" in diameter. The neutrons are detected in the ${}^6\text{LiI}$ via the energy released in the ${}^6\text{Li}(n,\alpha){}^3\text{H}$ reaction. Once the moderated neutrons reach the scintillator, the light pulses from the thermal neutron interaction with ${}^6\text{LiI}$ are converted to an electrical signal and processed by the electronics to produce detector counts. The ${}^6\text{LiI}$ scintillator is a 4 mm by 4 mm right-circular cylinder designed to provide the best gamma-ray (γ -ray) discrimination due to the skin interaction probability of the thermal neutrons in the ${}^6\text{LiI}(\text{Eu})$ scintillator. In this configuration, 80% of incident thermal neutrons are detected in the first 1 mm of LiI (a surface effect), while fast neutron and γ -ray detection is proportional to the scintillator volume. This large surface-to-volume ratio reduces the number and maximum size of the detectable gamma pulses allowing excellent pulse discrimination (Bramblett, 1960). Figure 3 shows the comparison between a Pu-Be source with 0.6 gamma rays per neutron and a Ra-Be source which has approx. 30,000 gamma rays per neutron. Even in the presence of such a large number of gamma rays, the ${}^6\text{LiI}$ scintillator provides a well-defined neutron peak (Bramblett, 1960).

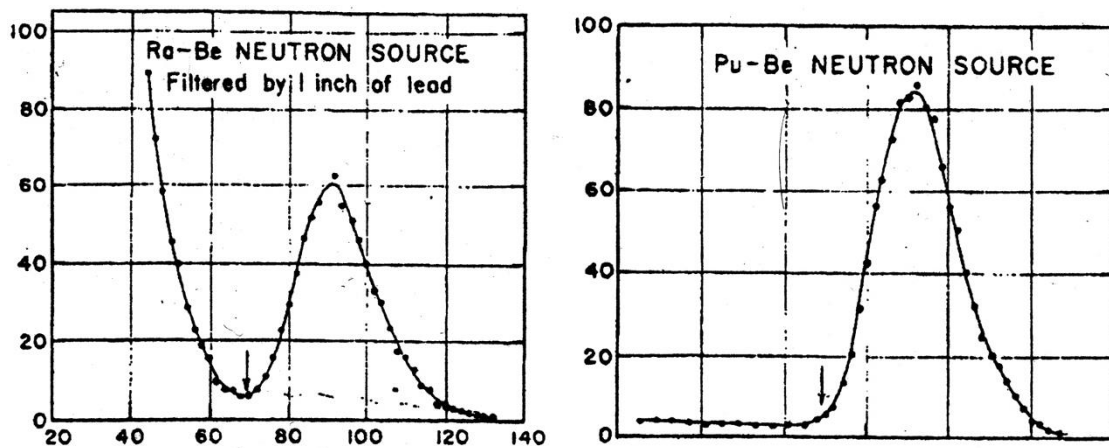


Figure 3: Evidence of gamma discrimination (Bramblett, 1960)

Bonner Sphere Extension (BSE)

Since Bonner spheres detect moderated incident neutrons, it is possible to increase the effective range of neutron energy that can be detected by increasing the moderation. If larger HDPE spheres are used to increase energy range, it would be at the cost of drastically reduced efficiencies (Knoll). To maintain reasonable efficiencies, high-Z materials, *i.e.* materials with higher atomic number, can be used in conjunction with HDPE (Birattari, 2004; Burgett, 2008). These high-Z materials are selected for their large (n, xn) cross sections which cause them to release multiple (2 and greater) neutrons per single high energy neutron when the incident energy exceeds the reaction Q-value.

The combination of a sphere of high-Z material and a HDPE Bonner sphere for detection is referred to as a heavy moderator. Specific nomenclature for such spheres is “#XxY”, with the possible choices for each expressed in Table 2. For example a 3” Bonner sphere covered by lead and a HDPE shell will be abbreviated—3PbC.

Bonner Sphere (in)	High-Z Material (Xx)	Presence of HDPE Shell (Y)
3	Copper (Cu)	No (B)
5	Lead (Pb)	Yes (C)
	Tungsten (W)	

Table 2: Nomenclature of BSE assemblies

The heavy moderator assemblies function like the HDPE from a BSS with scatter, absorption, and moderation resulting in detection as shown in Figure 4 (Burgett, 2008). The heavy moderators allow for better count rates for higher neutron energies than HDPE (Hsu, 1994). The neutron energies produced in this work are lower than the Q-

value of the (n, xn) reactions. In this case the BSE spheres do little more than act as neutron moderators for this experiment.

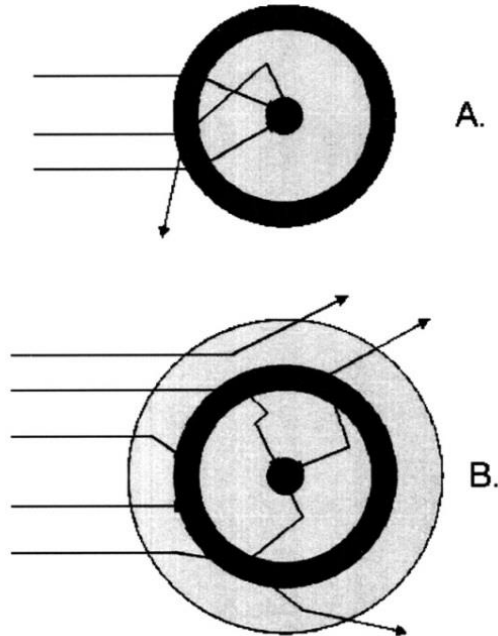


Figure 4: Schematic of neutron interactions in the BSE. The dark outer ring is the high Z-materials, with a thermal neutron detector at the center (Burgett, 2008)

One such extension of the standard Bonner sphere setup was developed by Burgett (Burgett, 2008). This BSE adds up to 18 additional sphere combinations and was developed for measurements up to 800 MeV, resulting in response functions optimized for higher energies (Burgett, 2008). There are three high-Z materials used in this extension, Copper (Cu), Lead (Pb), and Tungsten (W). Each of these materials is made in a 3" inside diameter (ID), 5" outside diameter (OD) shell and a 5" ID, 7" OD shell—exact measurements can be found in Table 11 of the Appendix. These shells are machined so that the smaller shell fits inside the larger shell, creating a nested-shell assembly with thicker high Z-material. There are HDPE shells for both the small and large diameter shells. The small HDPE shell has a 5" ID and 8" OD, and the larger shell has a 7" ID and a

12" OD. The completed small and large assemblies can be seen in Figure 5 (Burgett, 2008). The nested shells are used for high energy neutrons (>10 MeV) and were not used for this experiment.

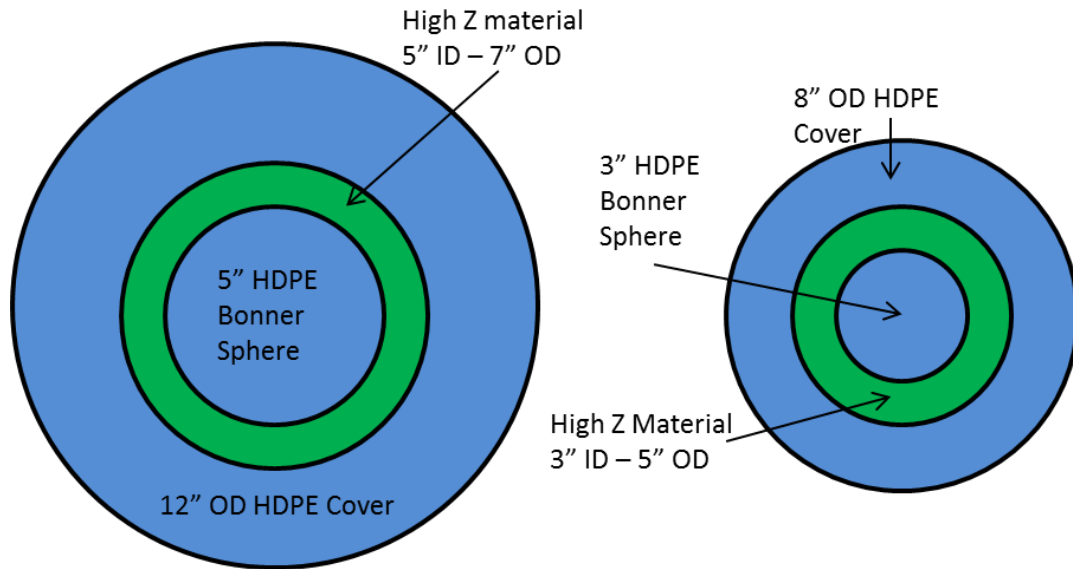


Figure 5: Cross section of the large and small assemblies

CHAPTER 2: Theory

Neutron Unfolding

To encompass the entire neutron energy range, BSS and BSE employ multiple spherical moderators placed with the scintillator at the center of each moderator. Since each moderator requires its own measurement, each moderator/scintillator combination is referred to as a detector. This results in detector spectra for 6 different moderators in the case of the BSS and at most 24 for the BSE. As there are fewer detectors than there are data points to describe the spectrum, no unique solution is possible making computer codes the best method of solving this underdetermined system of equations (Johnson, 1987).

A piece of software developed specifically for use with Bonner spheres is the Maximum Entropy Deconvolution program (MAXED). This software utilizes the relationship between counts (measured), the neutron spectrum (deduced) and detector response (known *a priori*). This relationship is a first order Fredholm integral equation, shown in Equation 1 below (Reginatto, 1998; 2004).

$$N_k + \epsilon_k = \int R_k(E)f(E)dE$$

Equation 1: First order Fredholm integral equation

N_k = number of counts measured by detector k

$R_k(E)$ = detector's response

$f(E)$ = neutron spectrum

ϵ_k = unknown measurement uncertainty

Each detector has an *a priori* response function (R_k) whose peaks and shape change with moderator size (Reginatto, 1998), and it is crucial to select the appropriate response function for the detector and measurement to avoid unnecessary errors in the resulting neutron spectrum (Thomas, 2002). Examples of response functions for a BSS are shown in Figure 2 and tabulated versions of these curves are required inputs into MAXED.

Since MAXED is designed specifically for use with Bonner spheres, the program allows the input of the known detector uncertainty (σ_k) and is carried throughout the deconvolution to predict the total uncertainty in the resulting neutron spectrum. MAXED is the preferred unfolding program because of the uncertainty propagation, as other spectral unfolding software have no uncertainty propagation.

The parameter Ω , see Equation 4, fixes the chi-squared statistic of the solution and a default spectrum (f_i^{DEF}) is input into MAXED for comparison using the maximized entropy expression in Equation 2.

$$Entropy = - \sum_i \left\{ f_i \ln \left(\frac{f_i}{f_i^{DEF}} \right) + f_i^{DEF} - f_i \right\}$$

Equation 2: Expression for maximizing the entropy

The MAXED algorithm can be simply described by a set of input and output parameters with a set of equations relating the parameters to one another (Reginatto, 2002). The MAXED parameters used in Equation 3 through Equation 7 are defined below.

N_k : measured counts of detector k

σ_k : estimated standard uncertainty of detector k

f_i : solution spectrum value for energy bin i

f_i^{DEF} : default spectrum value for energy bin i

R_{ki} : response matrix value for detector k and energy bin i

Ω : parameter that fixes chi-squared of the solution

ϵ_k : difference between predicted and measured value for detector k

The output is a set of parameters $\{\lambda_k, \gamma\}$ that satisfies the following set of equations (Reginatto, 2002):

$$N_k + \epsilon_k = \sum_i R_{ki} f_i$$

Equation 3: Summation notation of the Fredholm integral in Equation 1

$$\sum_k \frac{\epsilon_k^2}{\sigma_k^2} = \Omega$$

Equation 4: Constraint for handling ϵ_k

$$\sum_k \frac{N_k}{\sigma_k} - \sum_{k,i} \frac{R_{ki} f_i}{\sigma_k} = 0$$

Equation 5: Constraint on admissible solutions

$$f_i = f_i^{DEF} \exp \left\{ - \sum_k \left(\lambda_k + \frac{\gamma}{\sigma_k} \right) R_{ki} \right\}$$

Equation 6: Expression for solution spectrum in terms of $\{\lambda_k, \gamma\}$

$$\epsilon_k = \frac{\lambda_k \sigma_k^2}{2} \left(\frac{4\Omega}{\sum_j (\lambda_j \sigma_j)^2} \right)^{1/2}$$

Equation 7: Solution for ϵ_k in terms of $\{\lambda_k, \gamma\}$

Equation 3 through Equation 5 are constraints on the permitted solutions while Equation 6 and Equation 7 are expressions for the solution spectrum. Any change in the input parameters causes the output parameters to change which lead to changes in the calculated f_i and ϵ_k . The Appendix of the “Unfolding with MAXED and GRAVEL (UMG)” manual discusses the linear algebra operations used to reach a final solution from MAXED (Reginatto, 2004).

Each measurement distance is unfolded through MAXED using an iterative process. The unfolding begins by including only the BSS data. After the first iteration, each successive iteration adds only one BSE sphere’s data to the BSS data until each BSE sphere’s data has been included with the BSS data. For each iteration, the chi-squared value for the solution is calculated by MAXED and compared to the user defined limit. This limit on chi-squared is set to prevent the algorithm from diverging. Once the minimum chi-squared values for the solution spectrums are found, the data is run through MAXED again. Running the data one more time to match all the chi-squared values between iterations for the solution spectra (f_i), *i.e.* the neutron energy spectra, allows for the best comparison between each BSS + 1 BSE sphere iteration for a given measurement distance.

CHAPTER 3: Experiment

Physical Setup

This experiment was setup inside the shielding walls around the Pelletron target section—see Figure 6. The walls extend from the end of the 25 foot Pelletron tank to about 8 feet from the overhead door. These walls are built of solid concrete blocks (6'x2'x2' each) with a thin layer of borated polyethylene facing the target and are placed 7' apart. The target section is at the end of the beamline that extends over 8' from the high energy exit of the Pelletron.

The ^6LiI scintillator was set at the center point of the exit port of the Pelletron using a theodolite, with the assistance of Todd Gansauge, and points were marked along the floor of the measurement room along the center line at 1, 2, 3, and 4 meters. Measurements were taken from the target and sidewalls to centerline of the ^6LiI detector without any moderators present to ensure proper detector placement at each location and to be able to reproduce the detector location for follow-up neutron measurements. At each location a measurement was taken for each sphere configuration excluding the bare detector and the nested metal hemispheres.

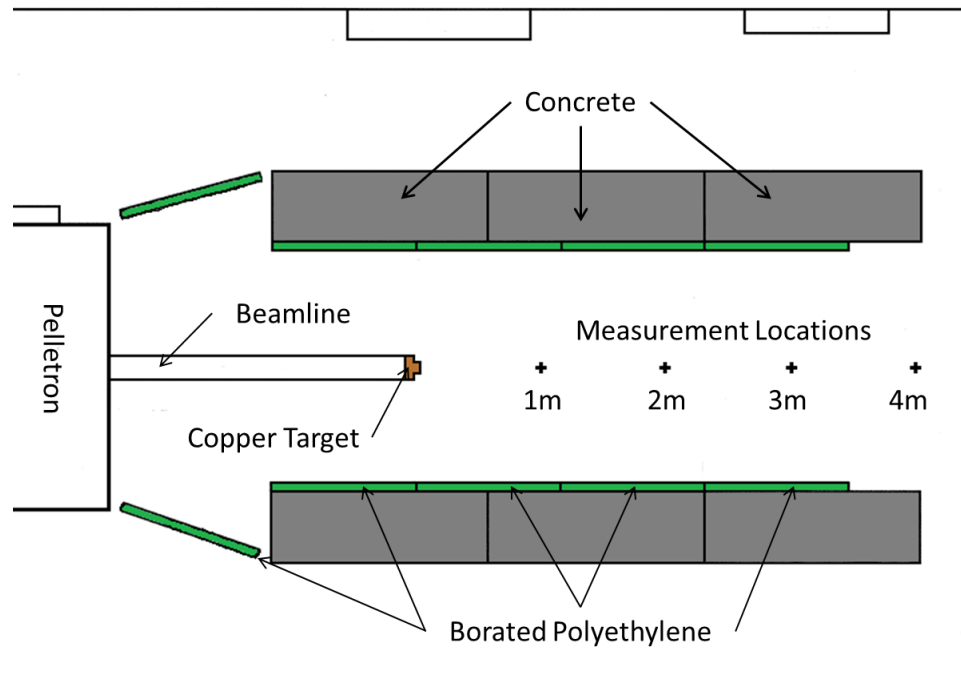


Figure 6: Excerpt from shielding diagram for Pelletron

Measurements were taken for neutrons produced by the Pelletron via the proton interaction with the copper target and for neutrons from an Americium-Beryllium neutron source ($^{241}\text{Am-Be}$). The $^{241}\text{Am-Be}$ data provides a reference spectrum for comparison to measurements taken at other facilities with a $^{241}\text{Am-Be}$ source. This allows the calibration factor of the Model 42-5 Bonner spheres from Ludlum Instruments to be determined (Ludlum, 2015). In order to maintain the effect of the room geometry on this measurement, the $^{241}\text{Am-Be}$ source was mounted flush with the end of the copper target and because of the beam line the closest mounting position was 13.5 cm (center to center) above the target.

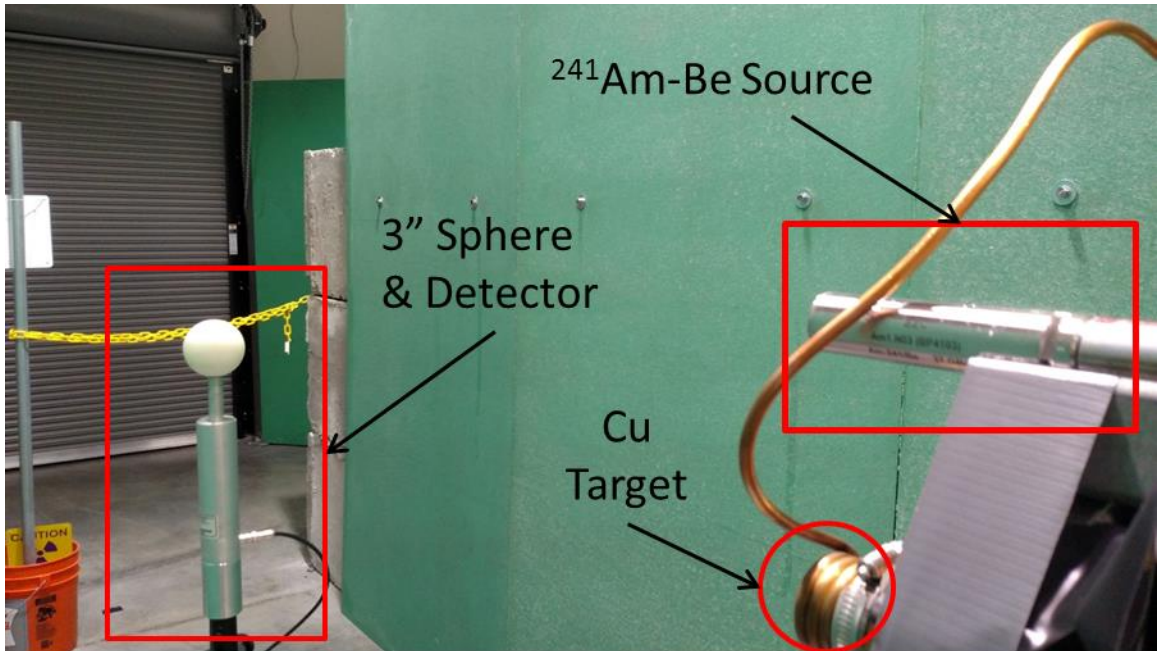


Figure 7: Physical Setup of detector in relation to target and $^{241}\text{Am-Be}$ source

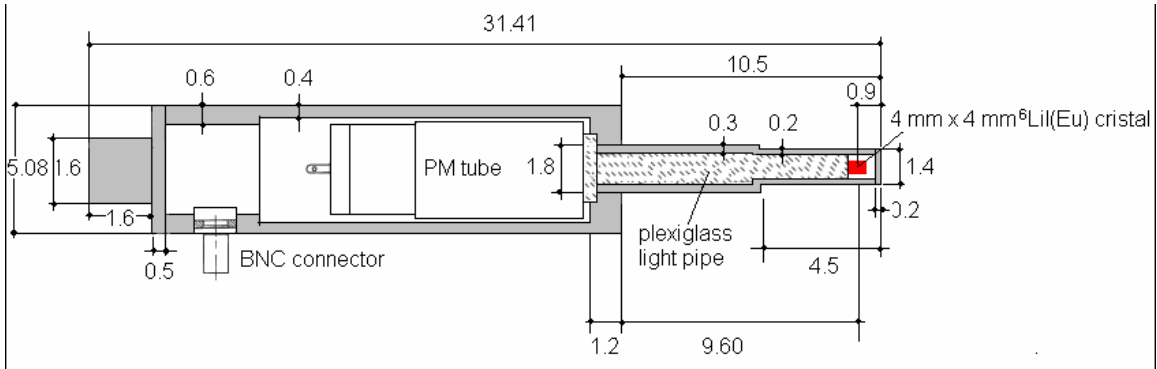


Figure 8: Schematic of detector internals and dimensions (Cruzate, 2007)



Figure 9: HDPE Bonner spheres



Figure 10: BSE hemispheres: copper (bottom), lead (middle), tungsten (top), HDPE covers (right)

Detector Setup

The ${}^6\text{LiI}$ detector triggers on the thermal neutron interaction with the ${}^6\text{LiI}$ to produce light pulses, as previously described. The pulses travel down a light pipe and into a magnetically shielded photomultiplier tube (PMT) (Ludlum, 2015) which converts the photons into an electrical signal. These pulses travel through a series of electronics—see Figure 11, to manipulate the pulse into the proper readout for the Ortec Maestro program. The signal exiting the PMT enters an Ortec 142-IH preamplifier (preamp) which is mounted on the stand supporting the detector. This preamp is designed to decouple the high voltage from the detector and to amplify the signal from the detector while maintaining the signal-to-noise ratio and can integrate the charge in the pulse coming from the detector. The “Ortec Preamplifier Introduction” covers the basics in the signal processing and amplification of a charge sensitive preamplifier like

the 142-IH (“Preamplifier Introduction”). The “energy” output of the preamp travels along a 50 foot cable out of the measurement room and into an Ortec 572A Amplifier. This model amplifier allows for coarse and fine gain control, shaping time, a baseline restorer with discriminator, and pole-zero adjustments, while also supplying the preamp with power (Ortec 572A Manual). All of these parameters were fine-tuned while receiving pulses from the Lil detector to ensure the proper signal reaches the final stage. The unipolar output from the amplifier then travels into a multichannel analyzer (MCA) which connects directly to the computer via USB and interfaces with Ortec’s general purpose MCA software, Maestro. Maestro then records the pulses it receives (0-10V), with each pulse being a count and the voltage of that pulse relating to the particle energy. Because Maestro utilizes only voltage and counts, it is possible to setup for a wide variety of energy ranges. In this particular case, the linear amplifier was calibrated such that the neutron peak registered around 2-4V as read out in the Maestro software toolkit.

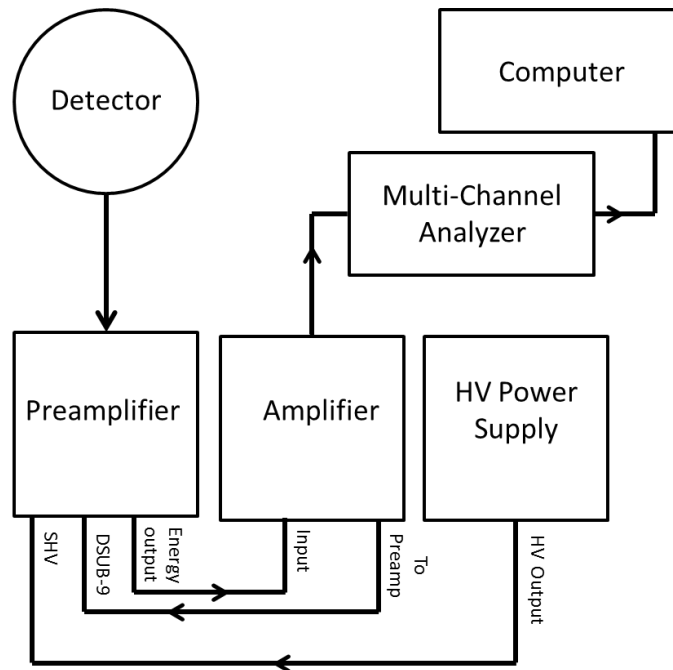


Figure 11: Setup of electronic modules



Figure 12: Picture of electronics and computer interface

Pelletron Setup

Understanding the process of recording the neutron data is important, it is also necessary to understand the source of the neutrons. Neutrons being measured by the BSS (and BSE) were produced using a Pelletron (Model 12SDH-4) manufactured by National Electrostatics Corporation (NEC). The Pelletron is an electrostatic tandem type accelerator capable of up to 4 million volts (MV) with relatively simple setup and operation. The accelerator consists of “a pressure vessel, a high voltage insulating support structure (referred to as the ‘column’), a charging system to generate the high potential, and an evacuated acceleration tube” (NEC, 2005). For acceleration, negative ions are produced and injected into a low energy tube where they are steered by a mass analyzing bending magnet, several electrostatic dipoles and quadrupoles while being attracted to the positively charged high voltage terminal. Four chains carry positive charge from the ground end to the terminal and negative charge from the terminal to ground resulting in the positively charged terminal needed for acceleration shown in Figure 13. The terminal is where the negative ions are stripped of electrons to become positively charged particles before being accelerated again due to electrostatic repulsion by the positively charged terminal (NEC, 2005). These positively charged particles are focused by a high energy quadrupole at the target end of the accelerator. The protons interact with the target to generate neutrons. The energy of the neutrons created is dependent on the terminal voltage of the Pelletron and the target material.

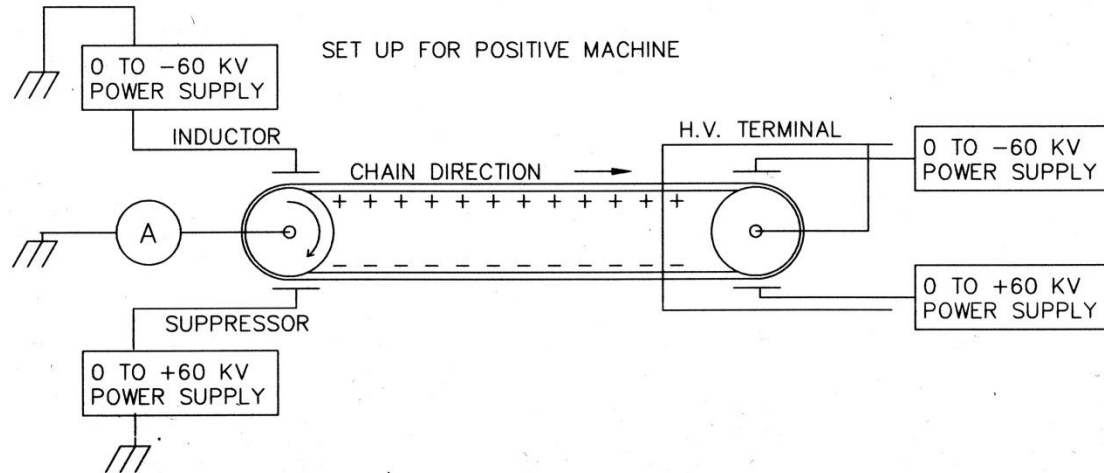


Figure 13: 4 MV charging schematic for Pelletron (NEC, 2005).

The target for the Pelletron is currently made out of copper for its superior heat transfer properties, but any suitable target material can be used in place of copper. There are two main criteria for selecting a target material. The first is the material's cross section which is the probability of a reaction, in this case (p, n), under specific conditions. Second is the ease with which the material can be handled, both before and after irradiation because some target materials react violently while others remain activated for long periods of time. Copper was selected for its machinability, excellent heat transfer and low activation probabilities. The schematic for the target is shown in Figure 14.

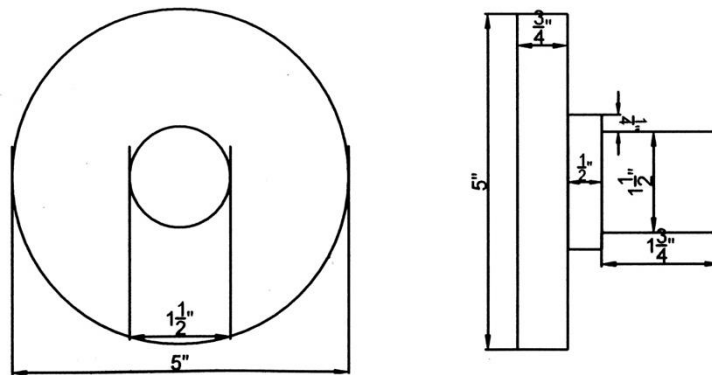


Figure 14: Copper Target Schematic a.) front view b.) side view

The type of copper selected is 99.9% pure, with the remaining 0.01% comprising lead, bismuth, oxygen and other contaminants (McMaster Carr, 2016). There are two naturally-occurring isotopes of copper, ^{63}Cu and ^{65}Cu and both have (p, n) reactions, but require very different minimum energies for neutron generation, referred to as the Q-value. The Q-value for ^{63}Cu is -4.148 MeV, while ^{65}Cu is -2.134 MeV (Soppera, 2012). Therefore, the terminal voltage of the Pelletron will determine which isotope of copper is responsible for the neutron production.

The Pelletron software contains a control algorithm that can maintain the terminal voltage and for this work was set to within 10% of a specified value. This feature was used to keep the terminal voltage at approximately 1.670 MV except during parts of the 1 meter measurement, where the control feature failed to adjust. Terminal voltage of 1.67 MV results in incident protons of approximately 3.3 MeV. This means that the neutron production is a result of the ^{65}Cu (p, n) reaction (Figure 15), with a cross sectional value of about 50 millibarns at an incident energy of 3.3 MeV. The proton energy of 3.3 MeV and the reaction's Q-value of -2.134 MeV results in a maximum neutron energy of about 1.17 MeV, with slight peak variations caused by fluctuations in the terminal voltage from the control software and CSDA range energy changes in the proton energy.

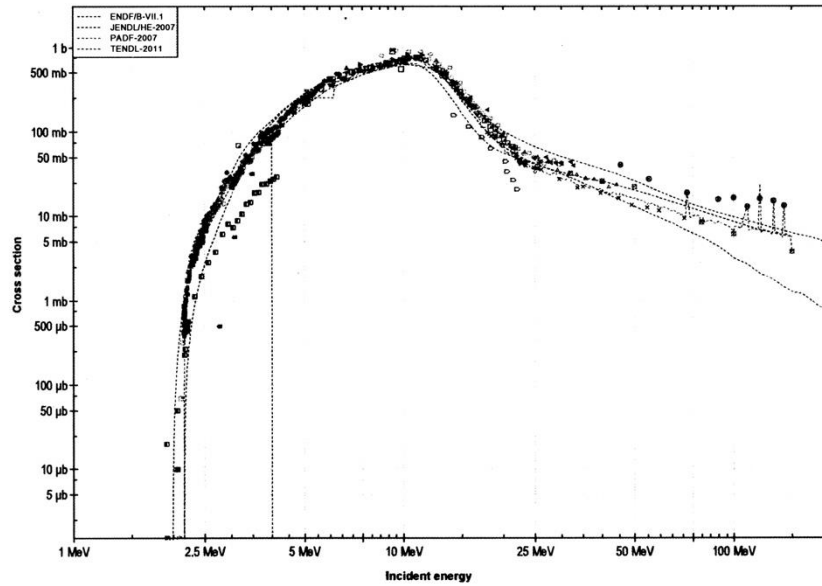


Figure 15: ^{65}Cu (p,n) cross section.

For this experiment the current was initially set so that the neutron dose in the surrounding rooms did not exceed 4 millirem per hour (mrem/hr) because at 5 mrem/hr the accelerator automatically shuts down to prevent excessive dose to the control room's occupants. The intensity of the Pelletron beam-current delivered to the target drifts as the H^- source warms up and is actively adjusted to keep the dose in neighboring rooms within limit. The variation of the current delivered to the target requires a recording of the current delivered for later analysis. A simple LabVIEW program from a previous project was used to record the current readout of a Keithley 485 Picoammeter in a data file with a time stamp. These data logs were stored for each measurement and were used later to normalize the detector counts to the current on the target. The current target file for the 5PbC sphere at the 3 meter location only recorded one data point so the 5PbC sphere data was not used in the unfolding of the 3 meter data.

The Maestro software was set to start recording first, then the LabVIEW program would begin recording data, and lastly the faraday cup would be removed from the beamline to allow the proton beam to impact the target. A timer was used to record the time that the beam was impacting the target, so the timer started with the removal of the cup and stopped when Maestro stopped counting. The LabVIEW program was stopped last, but since the current with and without the cup acting as a beam stop was very different, it was easy to discern when the beam was on the target, and in all cases the elapsed time from the data file agreed with the timer used.

Data Analysis

Maestro is used to obtain the raw detector counts that form the basis of the unfolding input for MAXED. Maestro measures counts and plots the counts on a scale of 0-10 V based on the voltage of the electrical signal received from the electronics. A higher voltage means more electrons are being produced in the PMT and results in a count farther along the x axis in Maestro. As more counts are registered in Maestro, peaks start to form, and in this case, these peaks relate to low energy noise, gamma rays, and neutrons detected. By selecting the neutron peak and setting it as the region of interest (ROI), the program gives additional statistics for that region. This additional information includes gross area, net area, uncertainty in the peak data, the peak locations, and detected counts per second. The net area with its corresponding uncertainty and the detector live time are recorded. If, for some reason, the peak shifts between measurements, the ROI can be relocated to encompass the entire neutron peak, however this happened only once during data collection

The measured detector counts were normalized to counts per millicoulomb (mC) of delivered protons on target to enable comparison between each measurement. To do this the data log for each sphere was loaded into a spreadsheet and binned. The current data at the beginning and end of the data file from when the cup was blocking the protons was removed. The last time stamp was changed to the recorded beam on target time so only current while the measurement was in progress impacts the results. The LabVIEW program recorded a current value in microamperes approximately every 15 seconds. This value was converted to amperes. Charge was calculated for each bin using Equation 8.

$$\text{Coulombs } (C) = \text{Amperes } (A) \times \text{seconds}(s)$$

Equation 8: The relationship between coulombs and amperes

The charge of each bin was then totaled to provide the total charge delivered during each measurement and converted to mC. The counts and uncertainty were then divided by the mC to provide neutron counts/mC of delivered proton beam.

The data input for MAXED is the input file for Bonner sphere unfolding (.ibu) whose format is specified in the manual (Reginatto, 2004). An example of the .ibu file is in Table 3. The input file has information that identifies the Bonner spheres as they are defined in the response matrix (column 1) and an integer typically used to define the sphere's diameter in Column 2. The remainder of the information is the counts (column 3), uncertainty (column 4), and uncertainties due to statistics as a percentage (column 5) and uncertainties from other causes as a percentage (column 6). A negative value in column 7 excludes that data from the unfolding, as seen for the 12" sphere in Table 3.

When considering the energy of the emitted neutrons from the (p,n) reaction on copper, certain spheres have a statistically small probability of measuring the neutrons as exhibited by the response function of the 12" sphere. The 12" sphere had a ratio of calculated response to measured response that was well outside the acceptable limits (greater than 20%). This was causing the remainder of the spheres to have a higher ratio as well. Once the 12" sphere was removed, the remaining sphere's ratios dropped to within $\pm 10\%$.

1 Meter Pelletron Measurements with Cu Target						
17	0					
2inch-y	2.0	1.315e+3	3.907e+1	1.0	3.5	1
3inch-y	3.0	2.487e+3	1.249e+2	1.0	3.5	2
5inch-y	5.0	4.639e+3	1.001e+2	1.0	0.2	3
8inch-y	8.0	2.913e+3	7.345e+1	1.0	0.2	4
10inch-y	10.0	1.580e+3	5.841e+1	1.0	0.2	5
12inch-y	12.0	6.854e+2	3.272e+1	1.0	0.2	-6
3cu-b-y	13.0	1.924e+3	6.762e+1	1.0	0.2	7
3cu-c-y	13.5	1.549e+3	6.294e+1	1.0	0.2	8
3pb-b-y	14.0	2.118e+3	8.875e+1	1.0	0.2	9
3pb-c-y	14.5	2.946e+3	1.117e+2	1.0	0.2	10
3w-b-y	15.0	1.900e+3	6.936e+1	1.0	0.2	11
3w-c-y	15.5	8.877e+2	3.700e+1	1.0	0.2	12
5cu-b-y	16.0	2.874e+3	1.116e+2	1.0	0.2	13
5cu-c-y	16.5	5.499e+2	2.589e+1	1.0	0.2	14
5pb-b-y	17.0	2.906e+3	6.331e+1	1.0	0.2	15
5pb-c-y	17.5	1.225e+3	5.631e+1	1.0	0.2	16
5w-b-y	18.0	2.667e+3	1.061e+2	1.0	0.2	17
5w-c-y	18.5	4.092e+2	1.869e+1	1.0	0.2	18

Table 3: .ibu file for MAXED. Column 3 and 4 are the detector counts and uncertainty, respectively

A second file is used to control the parameters of MAXED and is called the control file with an .inp extension. This .inp file specifies what file has the measured data and response functions, names the output file, the default spectrum, highest energy, the target chi-squared value, temperature and reduction factor, as well as the energy bin structure for the output file. An example is shown in Table 4.

1Meter.ibu	File with measured data
liiy.fmt	File with response functions (RF)
1m-7	Name of output file
flat2.flu	File with default spectrum (DS)
10.	Highest energy (use E units of RF)
100	Requested final CHI ² per degrees of freedom
1.0,0.85	Temperature, temp. Reduction fact.
2,2	1=4bin. 2=DS bins. 3=RF bins., 1=dF/dE.
1	2=EdF/dE
0	1 = scale DS
	0 = use the MAXED DS scale factor

Table 4: Control file (.inp) for MAXED. Column 1 are the parameters and Column 2 explain each parameter

For this experiment each measurement distance had its own .ibu file loaded with the counts/mC and corresponding measurement uncertainty. The response functions are the same ones used by Burgett for the original BSE project (Burgett, 2008). The output file names were selected to display the measurement distance and current iteration. The highest energy was set to 10 MeV, well above the expected 1.1 MeV peak. The chi-squared value is a parameter, Ω , that is set in the input file and fixes the chi-squared of the solution spectrum. The temperature and reduction factor were left at the default and the bin structure was set to 10 bins and then later to 4 bins to allow a cleaner graphical representation of the spectra.

MAXED outputs several different file formats with different information in each. The .plo output is used to plot the data in UMGPlot. This series of three plots contain important information about the unfolded neutron spectra, the effect each sphere had to the calculation and visually shows if the chi-squared limit was set too low. The .par and .flu outputs are the other two outputs and examples can be found in Table 9 and Table 10 of the Appendix). The .flu data is stored in a text file with well-defined columns. For this reason, the .flu file is the file that all of the data was taken from and

transferred to spreadsheets. The .par file is used in IQU_FC33, which is a part of the UMG unfolding package capable of calculating integral quantities and their uncertainty for the MAXED solution spectra. The .iqu output contains integral quantities for the energy bins from the response function as well as for user-defined energy bins along with corresponding uncertainty values

Figure 16 and Figure 17 are plots 1 and 3 in UMGPlot when the .plo output is plotted. Figure 16 provides useful information about the convergence of the MAXED algorithm. If the control value, the number of local minima and maxima, begins to increase rapidly as the step number increases, then the chi-squared limit is set too low. These two plots are examples of setting the chi-squared limit too low, in this case the acceptable limit was set to 1.0. As MAXED attempts to reach chi-squared of 1.0, it allows a greater variation in data from energy bin to energy bin as seen in Figure 17. Figure 17 is jagged, has a near-zero value for the intermediate energy bins, and has little agreement in bin value in the neutron peak. These reasons cause it to be a poorly defined neutron spectrum resulting from over iteration in MAXED as the algorithm attempted to reach the desired chi-squared statistic set in the .inp file.

To fix this, the chi-squared limit in the .inp file can be increased until the plot of the control value does not result in a rapidly increasing control value. Figure 18 depicts a proper plot of control value versus step number. The legend above Figure 18 lists two chi-squared values, the first one is the user defined limit set by the .inp file and the second value is the chi-squared calculated by MAXED. In Figure 19 notice the smooth

transitions from energy bin to energy bin and the well-defined spectrum across all the energy bins.

The red line in Figure 17 and Figure 19 is the default spectrum designated in the .inp file being plotted as a reference. MAXED utilizes the default spectrum in the calculation of the unfolded neutron spectra, as described in Chapter 2. A flat line as the default spectrum includes no *a priori* information and while not having this information may result in a higher chi-squared limit required, it also has the least impact on the unfolded spectra. The resulting unfolded neutron spectrum could then be seeded as the new default spectrum to reduce the chi-squared statistic and simplify the comparison conducted in MAXED, resulting in a more physically appropriate neutron spectrum (Reginatto, 1998; Johnson, 1987). Since the measured neutron spectrum is not complicated the additional *a priori* information is not required.

The .plo output has a third plot that shows the ratio of measured to calculated response with uncertainty (determined by MAXED) for each sphere. These ratios can be used to determine if a specific Bonner sphere is skewing the unfolded data, thus needing to be removed. This was the case for the 12" Bonner sphere, as mentioned previously.

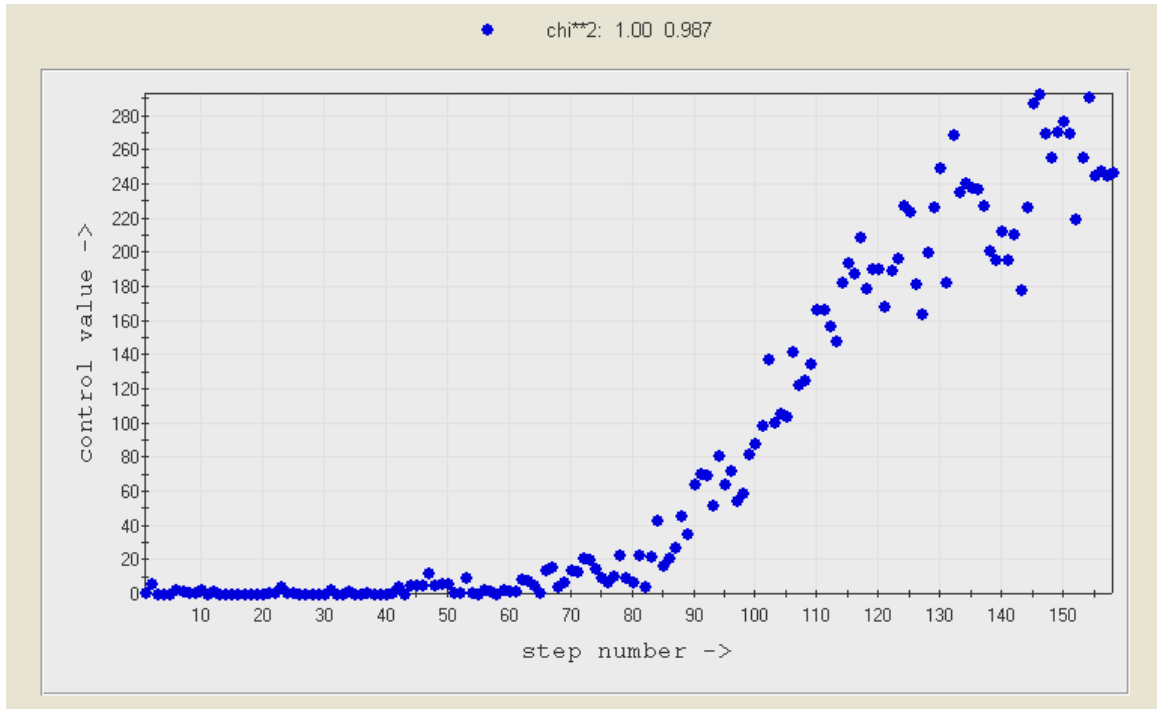


Figure 16: MAXED output (.plo) showing chi-squared limit is too low

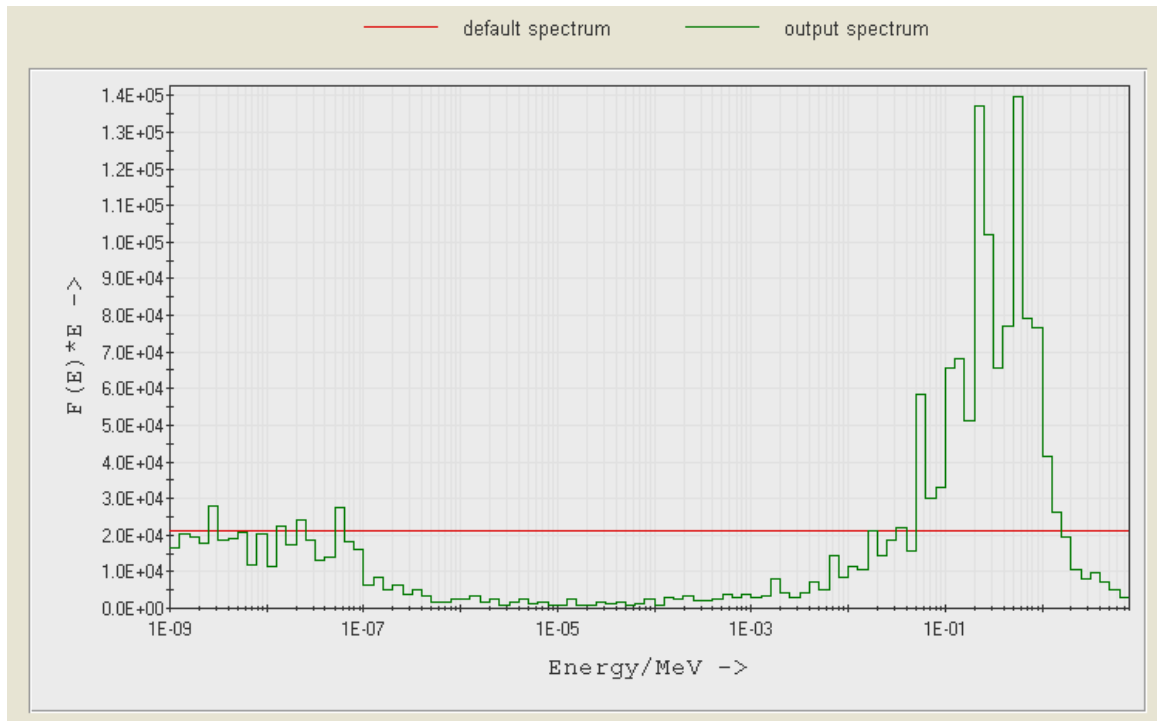


Figure 17: Plotted spectrum for over-iterated chi-squared

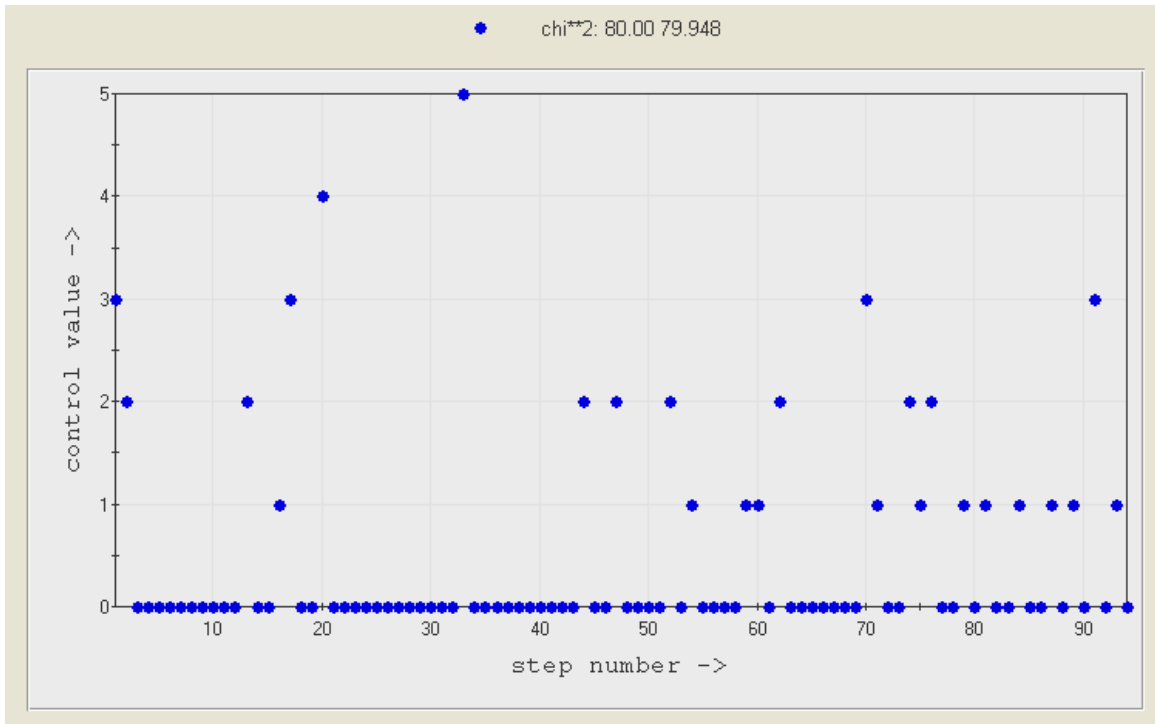


Figure 18: MAXED output (.plo) showing an acceptable value of chi-squared

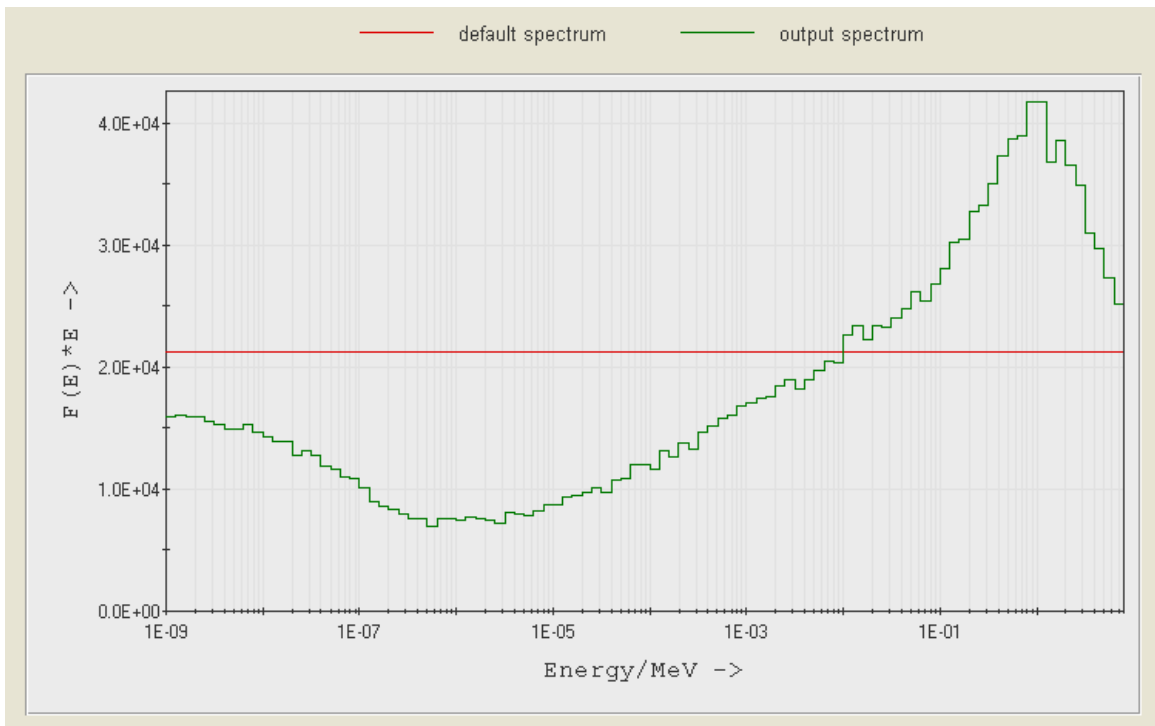


Figure 19: Plotted spectrum for a normally iterated chi-squared

The .flu output contains energy bin edge and value data. These files were loaded into a spreadsheet with the first two columns containing the data for the leading edge of the energy bin and the bin value. Because of the formatting of the .flu, the first column, the change in fluence per change in energy in units of $d\phi/dE$ was multiplied by the second column, bin energy, to match the units of $[E (d\phi/dE)]$ from UMGPlot. The data was then formatted so that the plots generated exhibit the bin structure rather than a smooth line. Figure 20 shows the .flu data spectrum plotted on the same scale as the UMGPlot spectrum, scaled by 1.1, to show that manipulated .flu data matches the solution spectrum from the .plo output. The actual UMGPlot of the .plo file is shown above in Figure 19.

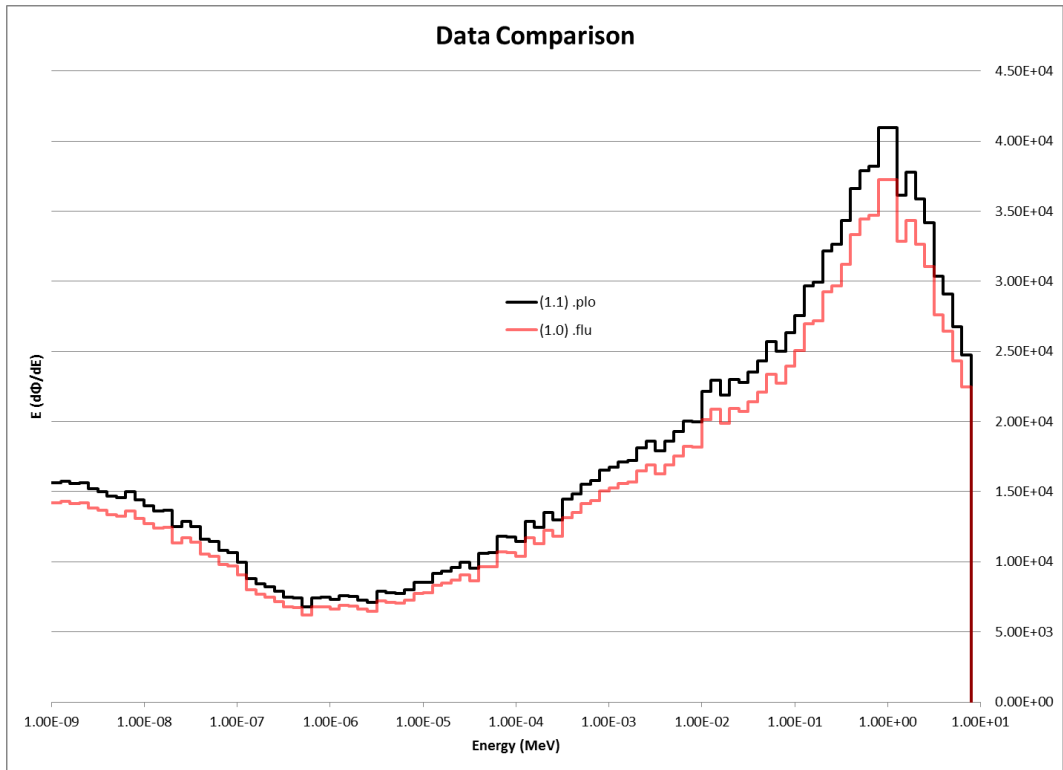


Figure 20: Comparison between .plo and .flu data plots

The $^{241}\text{Am-Be}$ source .flu data went through these same steps to reach a point where it could be plotted and compared to other $^{241}\text{Am-Be}$ data, except instead of counts/mC, it was normalized to counts/s. The data was collected only with the 6 BSS spheres because of the long count times to achieve <1% uncertainty in the detected neutron peak. The $^{241}\text{Am-Be}$ data underwent several additional calculations that were not possible with the Pelletron data. This analysis determines the contribution the room geometry and air scattering had on the final neutron spectrum. The $^{241}\text{Am-Be}$ data was used because there are multiple calibration spectra available for comparison, whereas there is little data available for comparison to the Pelletron data. The raw $^{241}\text{Am-Be}$ data underwent several calculations to determine correction factors for air in-scatter and room-return neutrons as prescribed by NBS special report No. 633 (NBS-633) (Schwartz, 1982).

The first correction is for air in-scatter. NBS-633 suggests that the detector counts increase due to air in-scatter by 1.7% and 1.0% per meter for 3" and 9" spheres, respectively. The neutrons that scatter in air will have a lower energy than the un-scattered neutrons, thus increasing the probability of moderation and detection for the smaller moderators. The BSS used here contains more spheres than those reported in NBS-633, the 2", 3", and 5" spheres are assumed to be approximate to the 3" sphere reported. This approximation is based on the similarities in the response curves of a 2" and 3" Bonner sphere (Figure 2). However the 5" sphere has little in common with either a 3" or a 9" sphere. The comparison to a 3" is taken as a worst case scenario. The data was not interpolated from the two data points available because there is no

clear relation between the response function peaks and the response curve widths span several decades of energy with substantial overlap with neighboring response curves. The 2", 3", and 5" sphere utilize the 1.7% factor while the 8" and 10" used the 1.0% factor again due to the similarities in response. To obtain values independent of the in-scatter caused by the room, the detector counts were decreased by these percentages (Schwartz, 1982)

The next correction is for room-return neutrons. Room-return neutrons are the neutrons that scatter off the surfaces of the measurement room, in this case the shielding walls and floor. The ceiling of the measurement room is thin steel decking and is about 6-7 times farther away than the shielding walls and is ignored. A monte-carlo simulation of the measurement room would provide an accurate account of room-return and could take into account the room surfaces in more detail, however this work exceeded the scope of the project. Generally room-return neutrons are measured experimentally using a shadow cone. A shadow cone could not be obtained within the timeline of this experiment, but is slated for future work. Currently the room-return neutron contribution is approximated.

The Pelletron shielding configuration requires the room-return correction to be calculated for the case of multiple concrete surfaces. If the data corrected for air in-scattering is used and since room-return fluence is uniform and varies as $1/r^2$, the general equation for the total response, D is (Schwartz, 1982):

$$D \equiv R_o + R_r = \frac{D_o}{r^2} + R_r$$

Equation 9: Total response for room-return correction

D_o is the response to source neutrons only

R_r is the response of the detector to reflected neutrons

R_o is the response of the detector to the source neutrons

r is the source to detector distance

This equation can be simplified further as shown in Equation 10. In Equation 10 if Dr^2 is plotted as a function of r^2 then a straight line fit will give D_o as the intercept of that fit and D_oS will be the slope, with S defined by Equation 11.

$$Dr^2 = D_o(1 + Sr^2)$$

Equation 10: Simplified equation for determining D_o

Where S is the quantity for fractional room-return correction at unit source-detector distance (Schwartz, 1982) and is defined in Equation 11:

$$S \equiv 5.6g \frac{\sigma_r}{\sigma_o} \frac{4\pi}{\sum A_i}$$

Equation 11: Equation for fractional room-return correction

5.6 is a numerical value for the effective albedo for all of the reflecting surfaces

g is the factor that accounts for any anisotropy in the detector

σ_r is the spectrum averaged response to the reflected neutrons

σ_o is the spectrum averaged response to the source neutrons

ΣA_i is the summation of the neutron reflecting surface areas A_i .

For this calculation, D_o and σ_r are the unknowns. The BSS/BSE is isotropic so g is equal to 1; ΣA_i is calculated from the dimensions on the shielding drawing with 3 surfaces, the two side walls and the floor. The ceiling is ignored because the source to surface distance is 6-7 times that of the shielding walls. The values for σ_o , for each BSS sphere, were taken from calibration data in the International Atomic Energy Agency (IAEA) Technical Reports Series 403 (IAEA, 2001). The report contains data from Physikalisch-Technische Bundesanstalt (PTB), where a series of ^{241}Am -Be measurements were conducted and the values of σ_o , σ_r , and σ_T , were reported. Because σ_r and σ_T are the measurements with (σ_r) and without (σ_T) shadow cones, respectively, these values are a function of the measurement room's neutron-reflective surfaces and will not be the same as the values for these measurements. However, σ_o , is calculated by the difference between σ_r and the total response, σ_T , and is a function of the source strength and energy making it the best approximation for an otherwise unknown variable. Also, the PTB experiment used a 6" Bonner sphere, whose response is similar to a 5" Bonner sphere, so the σ_o was used interchangeably (IAEA, 2001).

Finally, if Dr^2 is plotted as a function of r^2 , see Figure 21, D_o can be determined and then applied to the slope value to solve for σ_r . The values for σ_r and D_o were then compared between the values calculated for counts corrected for air in-scatter and those that were uncorrected to determine the percent difference in the values and the effect that air in-scatter had on the results.

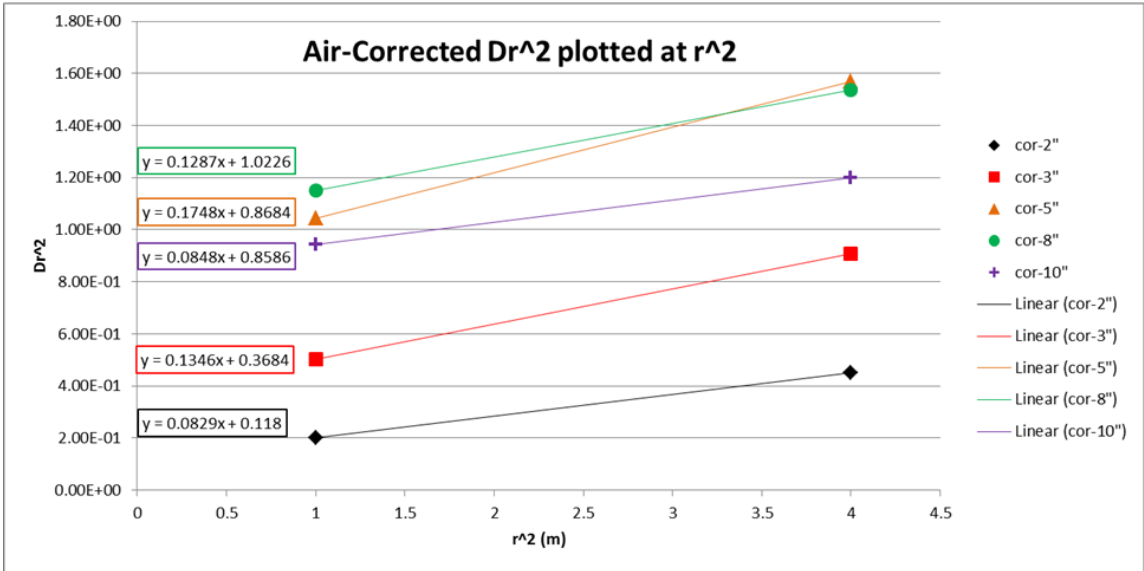
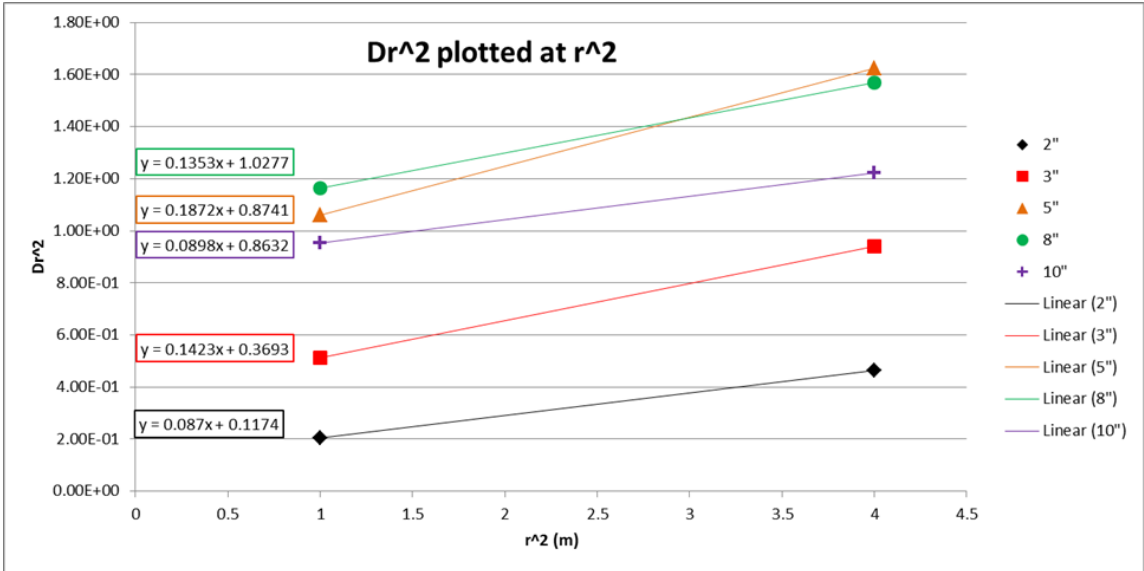


Figure 21: Dr² as a function of r² with corresponding trend lines

CHAPTER 4: Results

Plotting counts/mC as a bar chart and looking at the overall shape of the plot can give a preliminary indicator of detector counting error. The shape should resemble a normal distribution and any divergence can highlight anomalies in the detector data. Notice the peaks appear in the 5" spheres which suggests a neutron spectrum with more lower energy neutrons because the response curve for a 5" Bonner sphere peaks between 0.5 and 1 MeV. Table 13 through Table 17, in the Appendix, contain the detector count data and Pelletron settings.

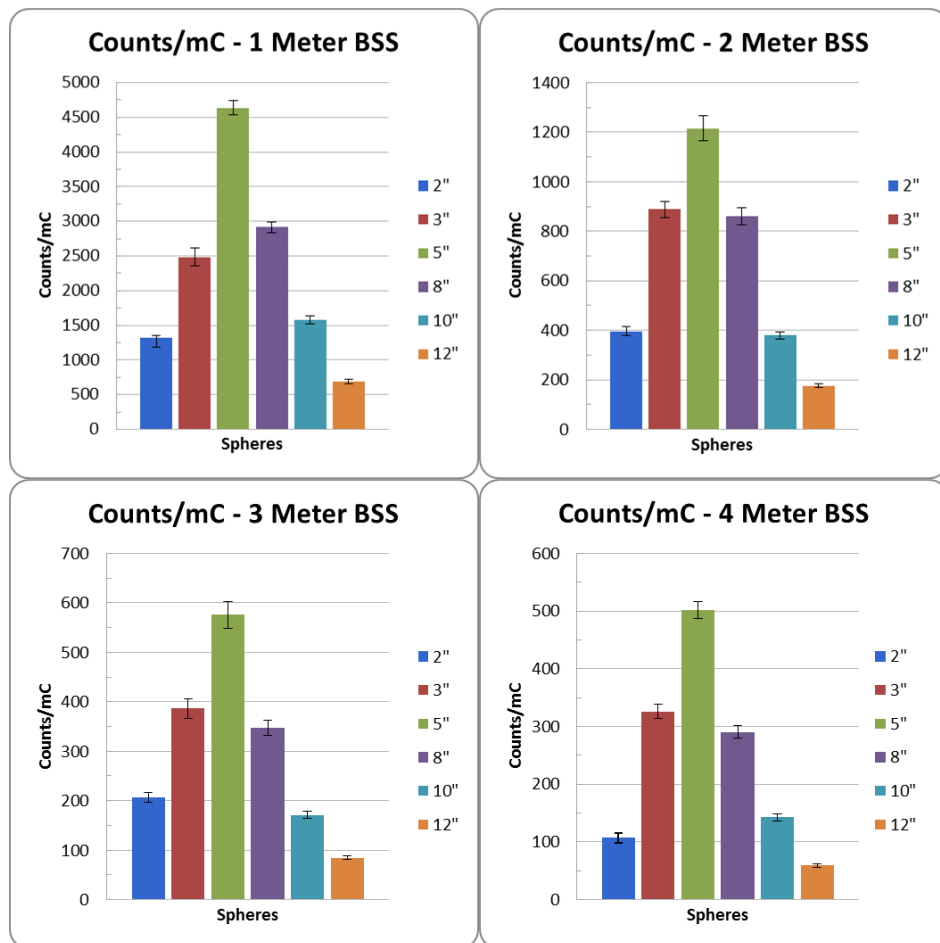


Figure 22: Plot of Count/mC for each BSS measurement distance.

The unfolded Pelletron spectra had an energy distribution and peak energy consistent with the Q-value of the reaction and the energy of the proton beam. An overview spectrum as measured by the BSS can be seen in Figure 23. Figure 24 through Figure 29 show the unfolded BSE spectra with peaks in the 1.0-1.1 MeV range. There is no BSE data for the 4 meter data because the beam time required to obtain <1.0% uncertainty in the detector was prohibitive. For the most part, the shape of the spectra stays the same across the measurement distances, only the intensity decreases as the distance increases. A more detailed breakdown of the unfolded spectra for the BSE can be found in Figure 37 to Figure 42 of the Appendix.

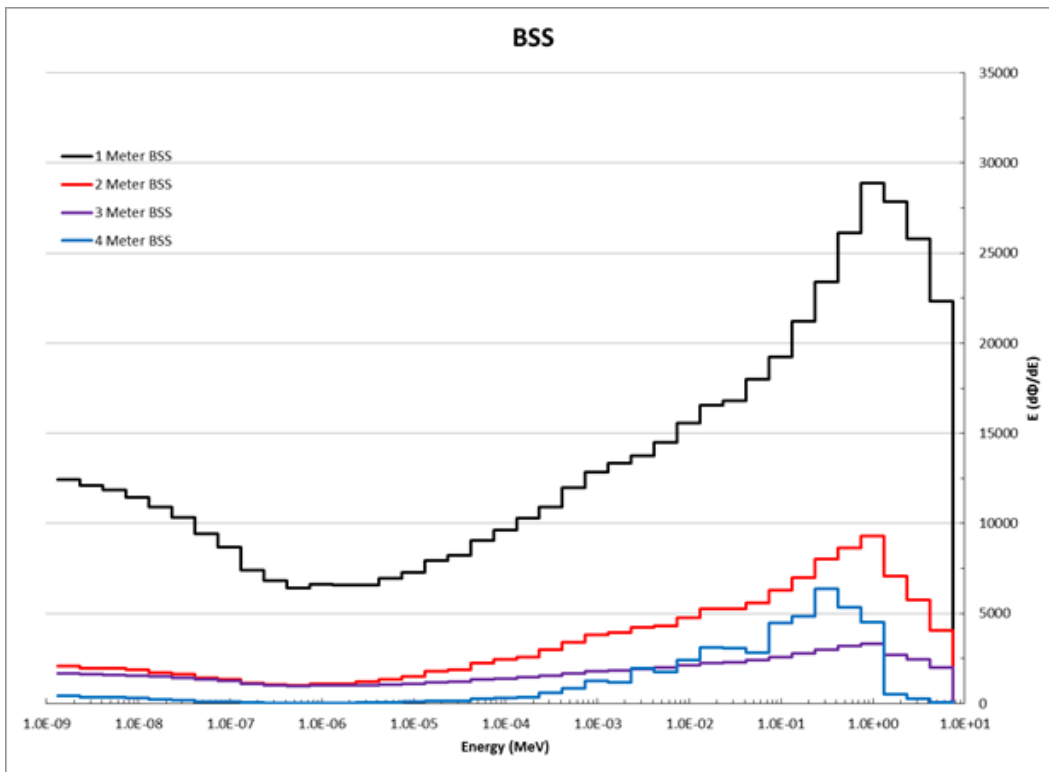


Figure 23: Plot of all the unfolded BSS measurements

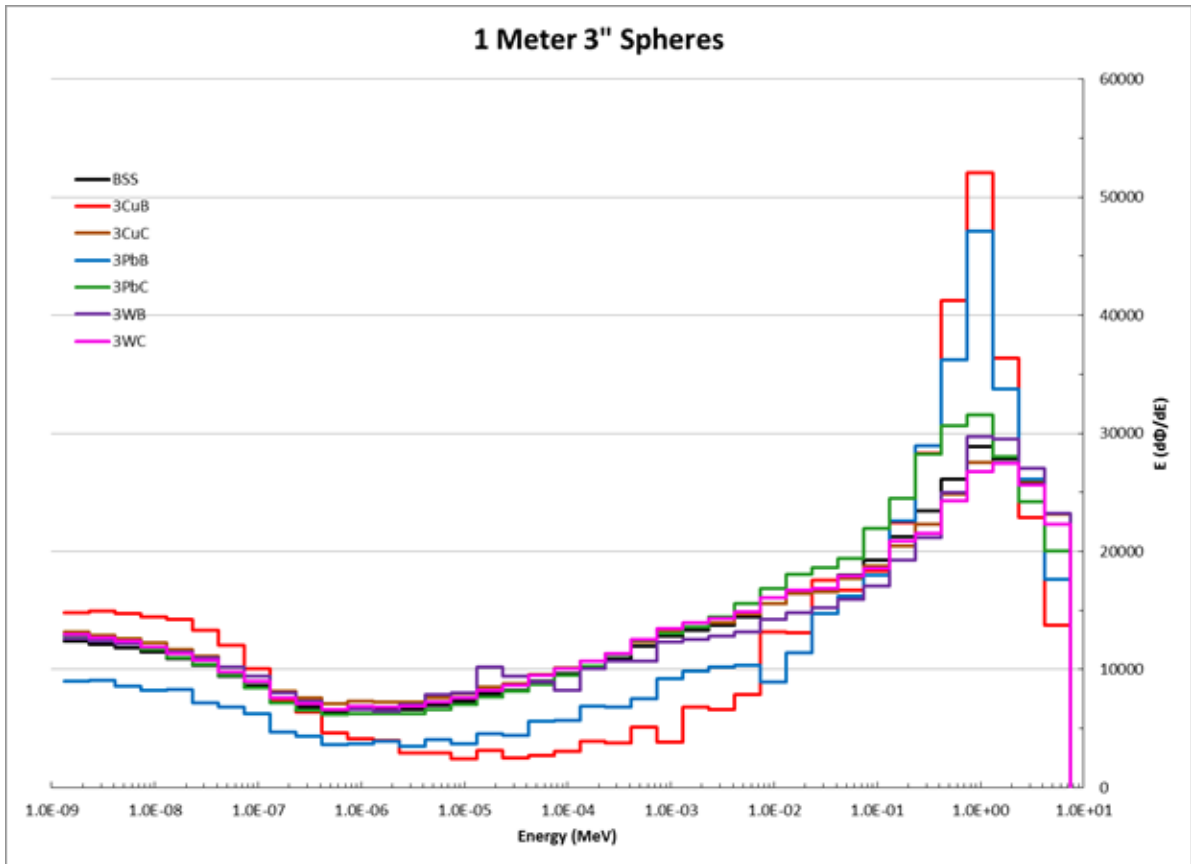


Figure 24: Unfolded neutron spectra for all 3" BSE spheres at the 1 meter location

In Figure 24 all of the 3" metal BSE spheres are displayed alongside the BSS measurement for the 1 meter location. This plot shows that many of the additional spheres very closely follow the unfolded spectrum from the BSS measurement. The 3CuB and 3PbB, however, have the same peak location but the peak intensity has a much higher value while the data from 0.1 eV to 10 keV in the unfolded spectrum is substantially lower than the results from the BSS spectrum. A higher intensity in an energy bin for one sphere, when compared to other spheres, suggests a difference in the response matrix for that sphere. In order to have any energy resolution, it is expected that certain spheres will result in more or less counts based on the peaks and valleys of the respective response curves for those spheres.

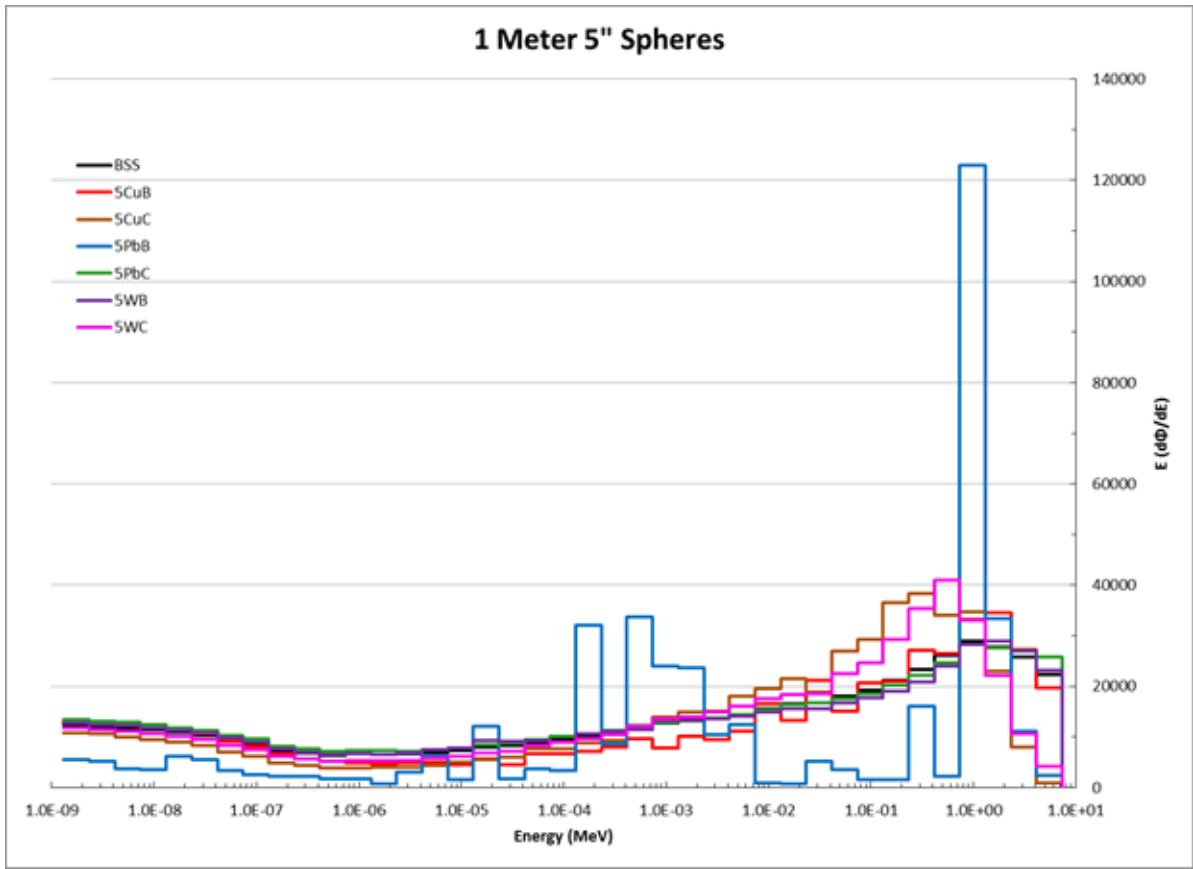


Figure 25: Unfolded neutron spectra for all 5" BSE spheres at the 1 meter location

Figure 25 shows the data for the metal spheres covering the 5" Bonner sphere. Again the bare lead sphere has the same peak location, but at a much greater intensity. The 5PbB spectrum fluctuates above and below the BSS spectrum for 1 meter and does not adhere to the same trend as the other metal spheres, which remain within +/- 50% of the BSS spectrum as seen in Figure 25.

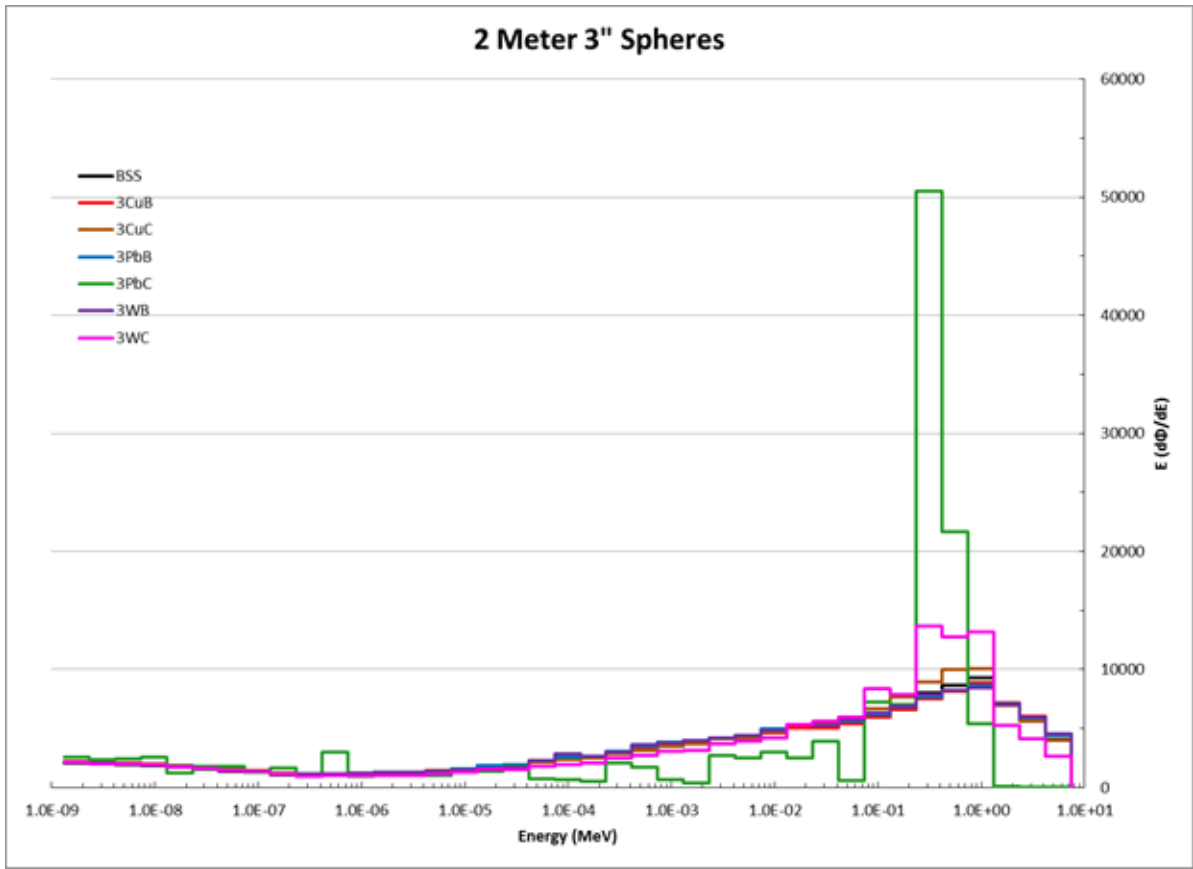


Figure 26: Unfolded spectra for all 3" BSE spheres at the 2 meter location

The bulk of the BSE spectra are within +/- 25% of the BSS spectrum except for the 3PbC whose peak is 5 times that of the BSS spectrum and the 3WC deviates slightly at the higher energies.



Figure 27: Unfolded spectra for all 5" BSE spheres at the 2 meter location

The spectra in Figure 27 are in excellent agreement with the BSS spectra. All of the lower energy spectra are within 30% of the BSS spectrum. Deviations from the 2 meter BSS spectra start to occur at the peak energy and higher with all of the covered spheres (5CuC, 5PbC, and 5WC).

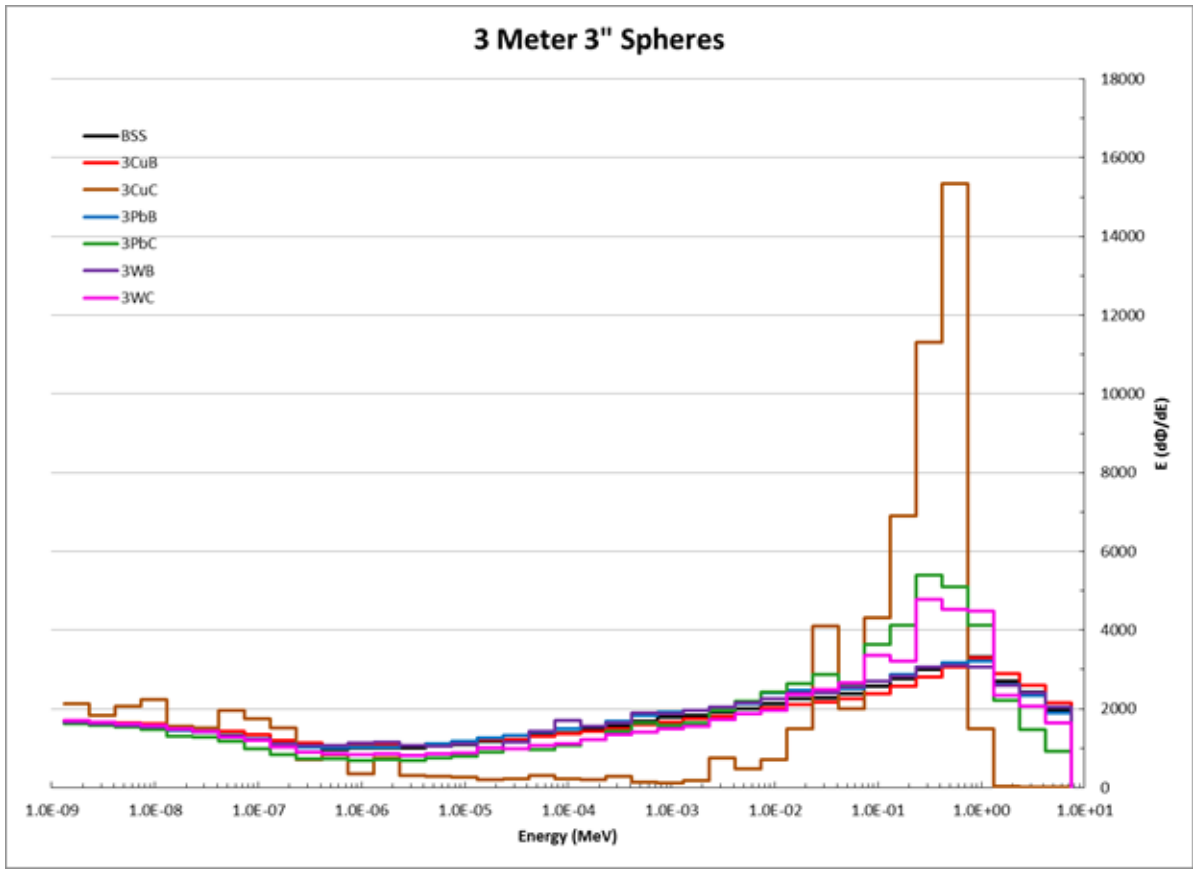


Figure 28: Unfolded spectra for all 3" BSE spheres at the 3 meter location

The 3 meter location spectra are also in agreement with the BSS spectrum. The only noticeable difference in BSE spectra is the 3CuC spectrum. This spectrum is nearly zero in the intermediate energies and above 1 MeV. The peak is shifted to a slightly lower energy than the rest of the data and the peak is 5 times that of the BSS spectra.

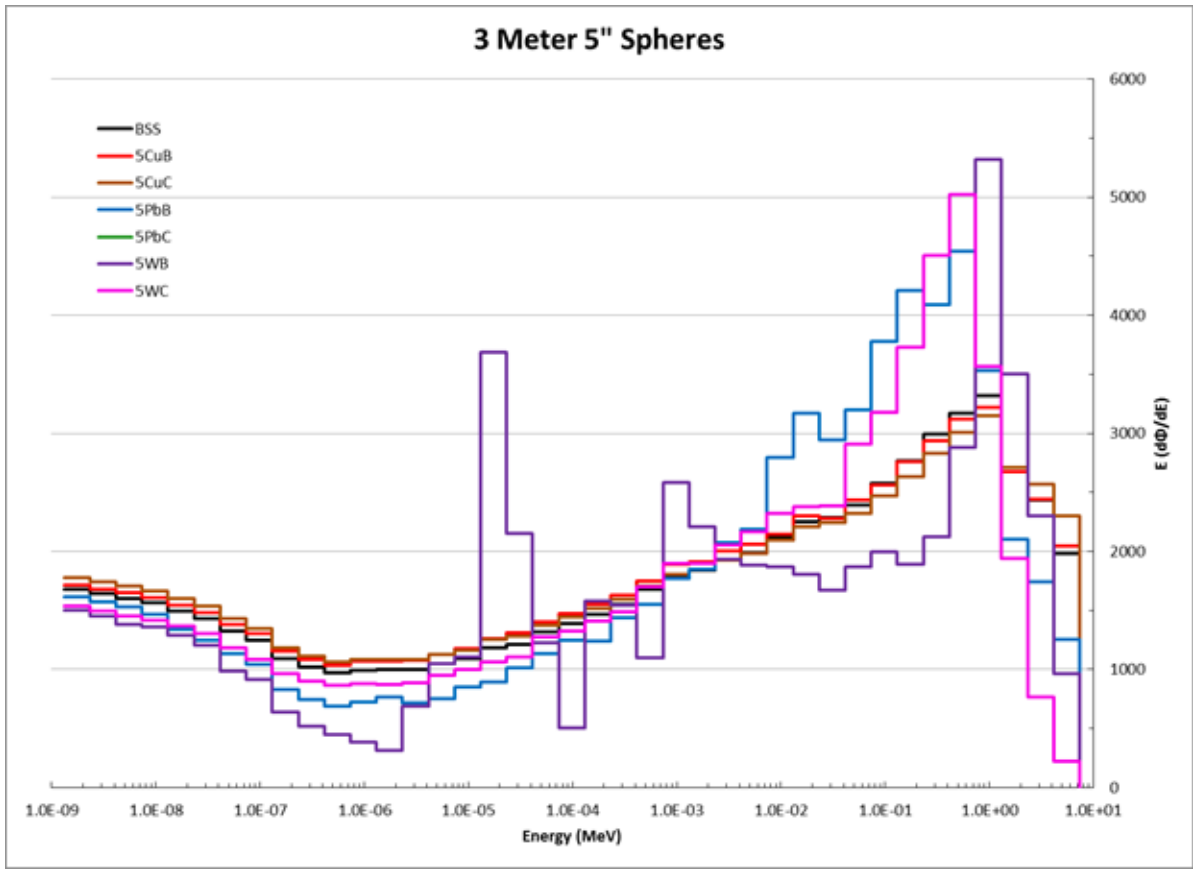


Figure 29: Unfolded spectra for all 5" BSE spheres at the 3 meter location

The spectra in Figure 29 have a similar shape as the BSS spectrum except for the spectra from the 5PbB and two tungsten spheres, 5WB and 5WC. All three of these spectra have a higher peak value and drop off much faster in the higher energy region above the peak.

Based on the comparison between the BSS and each individual BSE sphere, it is possible to calculate difference that each BSE sphere contributes to the resulting neutron spectra. These differences highlight which spheres contribute different counts in the Lil detector than the standard BSS spheres and at what energies this occurs. This information shows the effectiveness of BSE measurements at lower energy neutron fields. Variations in the data are expected as the response functions for each sphere are different. The plots for the percent difference in the 1 meter data comparison between each BSE sphere is shown in Figure 30 and Figure 31, while the remainder can be found in the Appendix starting at Figure 43. These plots highlight the differences in the response matrices for these lower energy neutrons.

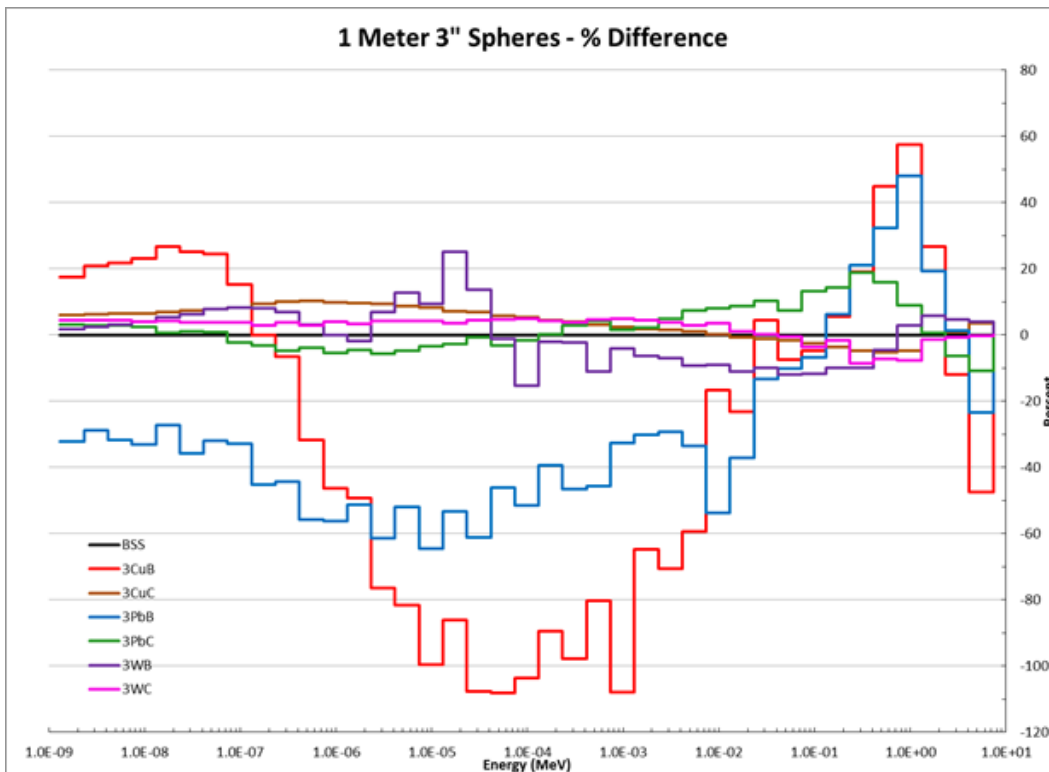


Figure 30: Percent difference in 3" BSE .v. BSS spectra at 1 meter location

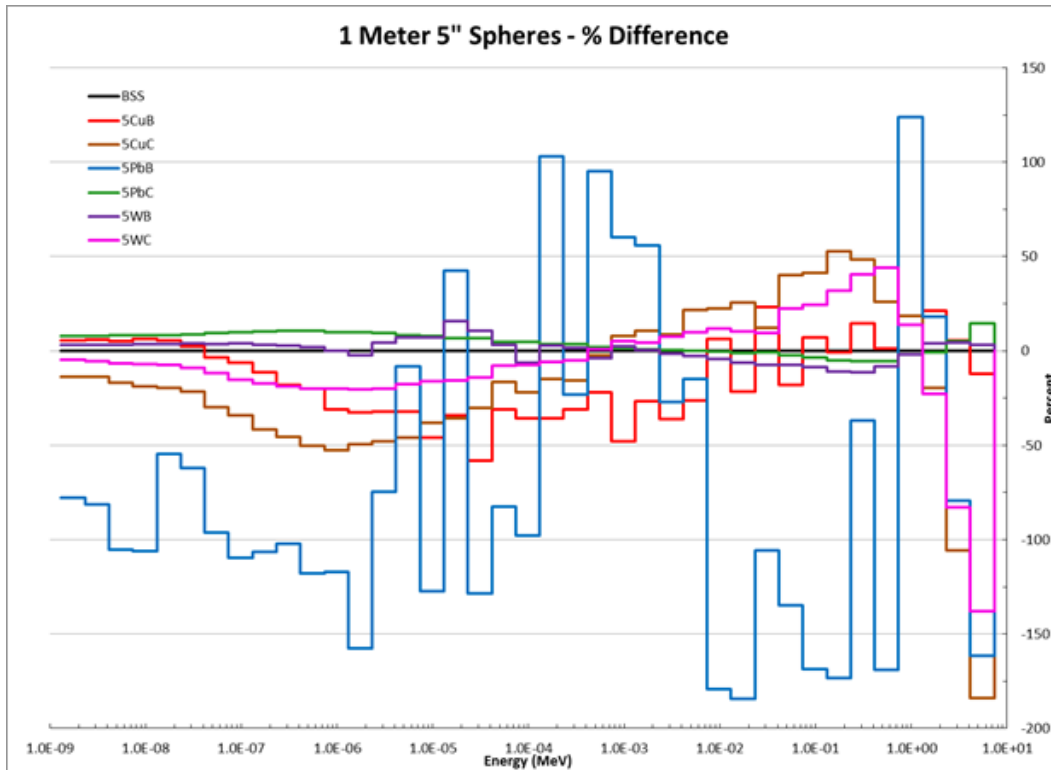


Figure 31: Percent difference in energy bins of 5" BSE and BSS spectra at 1 meter location

The .par file from MAXED was also used to calculate the integral quantities in user-defined energy bins using the IQU_FC33 program. This program provides the integrated fluence rate for a particular energy bin. In this case there are 3 energy bins. The low energy bin ranges from thermal energies up to 300 eV so that it encompasses the thermal, slow and resonant neutron energies. The intermediate energy bin ranges from 300 eV to 2.25 keV which is the energy for the unresolved resonance region of Uranium-235. An unresolved resonance region refers to the energies in a cross section just past the resonance region (energies with long-lived states of the compound nucleus) where minor resonance peaks can occur but cannot be measured by current techniques (Glasstone, 1967). And the fast energy bin ranges from the 2.25 keV energy to the upper limit used during the unfolding, which was 10 MeV. When looking at the tabulated data and plots, it is clear that little information about the neutron spectrum

was gained from the BSE spheres at the 2 meter location, but there were fluctuations in the resulting integrated fluence rate values at the 1 and 3 meter location. The flatness of each energy bin in Figure 33 shows that incorporating the BSE spheres into the standard 6 BSS spheres resulted in no new information about the original neutron spectrum.

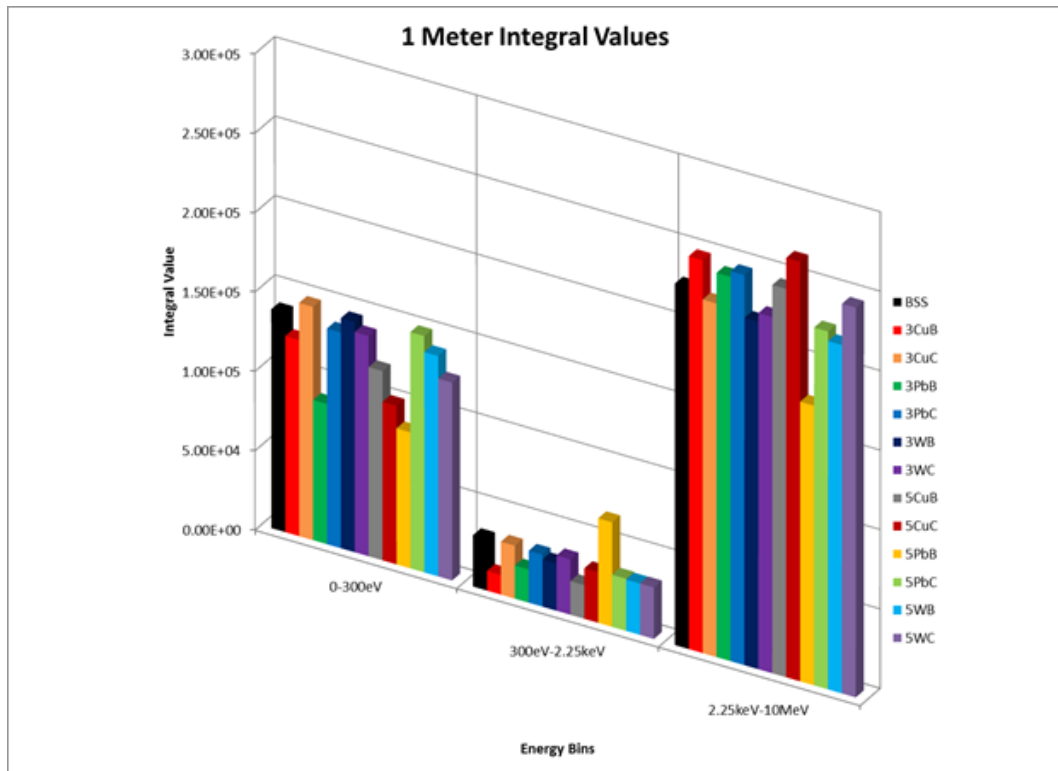


Figure 32: 1 meter integral values per bin for BSS and BSE

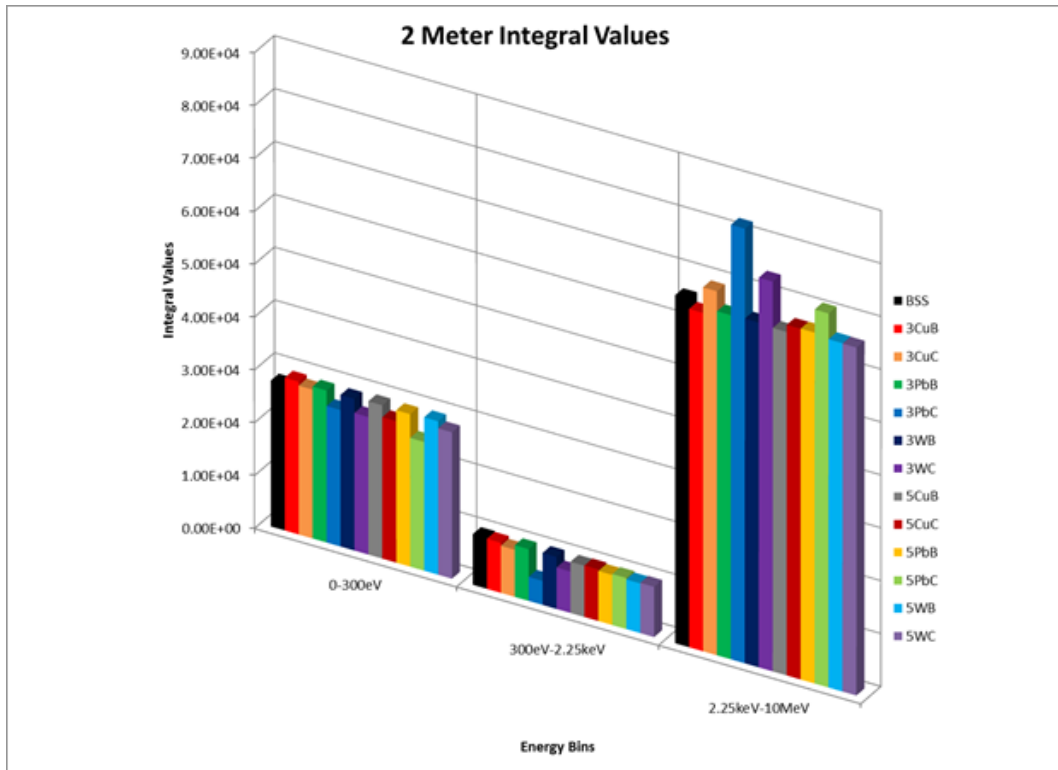


Figure 33: 2 meter integral values per bin for BSS and BSE

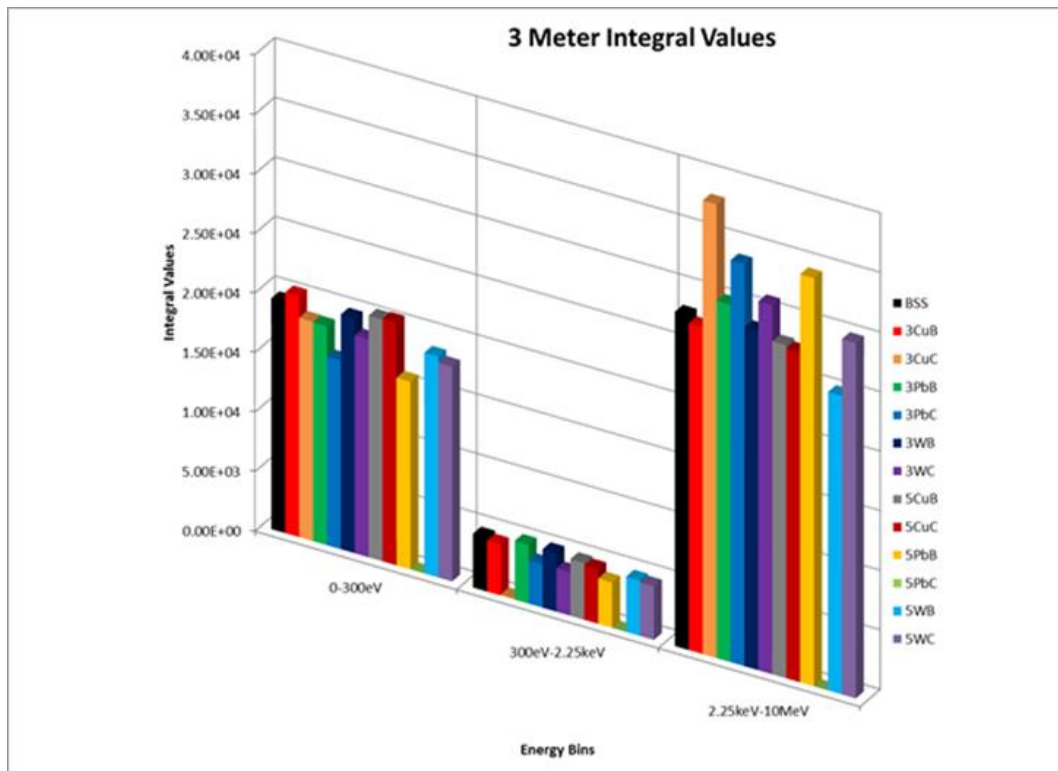


Figure 34: 3 meter integral values per bin for BSS and BSE

Figure 32 through Figure 34 show the values for the fluence rate in each of the three energy bins described. The 2 meter data in Figure 33 is the most consistent within each energy bin across all three bins for reasons not yet understood. The relative intensities between each bin at each location are similar and represent the consistency in the produced neutron field. Table 5 to Table 7 portray the data numerical and include a percent difference comparison in the integral fluence rate for the BSS spectrum and each BSE spectra.

1 Meter

Sphere	Integral Value			Percent Difference Integral Value		
	0-300eV	300eV-2.25keV	2.25keV-10MeV	0-300eV	300eV-2.25keV	2.25keV-10MeV
BSS	1.38E+05	3.24E+04	2.28E+05	---	---	---
3CB	1.24E+05	1.23E+04	2.47E+05	-11.033	-89.593	8.344
3CC	1.47E+05	3.33E+04	2.23E+05	6.341	2.916	-2.225
3PB	8.83E+04	2.08E+04	2.42E+05	-43.862	-43.302	6.116
3PC	1.36E+05	3.27E+04	2.46E+05	-1.512	1.002	7.599
3WB	1.45E+05	2.98E+04	2.19E+05	4.971	-8.258	-3.987
3WC	1.39E+05	3.49E+04	2.24E+05	0.580	7.420	-1.482
5CB	1.19E+05	2.12E+04	2.45E+05	-14.580	-41.716	7.144
5CC	9.99E+04	3.19E+04	2.64E+05	-32.011	-1.545	14.853
5PB	8.57E+04	6.59E+04	1.76E+05	-46.731	68.197	-25.520
5PC	1.49E+05	3.28E+04	2.25E+05	7.632	1.474	-1.023
5WB	1.39E+05	3.23E+04	2.19E+05	0.647	-0.102	-3.717
5WC	1.25E+05	3.25E+04	2.45E+05	-10.112	0.277	7.501

Table 5: 1 meter integral value data with comparison

2 Meter

Sphere	Integral Value			Percent Difference Integral Value		
	0-300eV	300eV-2.25keV	2.25keV-10MeV	0-300eV	300eV-2.25keV	2.25keV-10MeV
BSS	2.76E+04	9.61E+03	6.58E+04	---	---	---
3CB	2.89E+04	9.47E+03	6.40E+04	4.625	-1.494	-2.821
3CC	2.82E+04	8.91E+03	6.89E+04	2.042	-7.545	4.476
3PB	2.88E+04	9.78E+03	6.51E+04	4.089	1.731	-1.153
3PC	2.58E+04	4.55E+03	8.22E+04	-6.641	-71.463	22.107
3WB	2.87E+04	9.84E+03	6.52E+04	3.855	2.362	-0.944
3WC	2.60E+04	7.84E+03	7.37E+04	-5.870	-20.276	11.298
5CB	2.90E+04	9.70E+03	6.50E+04	4.974	0.930	-1.349
5CC	2.68E+04	9.76E+03	6.63E+04	-3.088	1.556	0.729
5PB	2.89E+04	9.49E+03	6.64E+04	4.443	-1.287	0.795
5PC	2.44E+04	9.66E+03	7.07E+04	-12.436	0.577	7.185
5WB	2.90E+04	9.40E+03	6.59E+04	5.042	-2.179	0.062
5WC	2.77E+04	9.52E+03	6.58E+04	0.363	-0.935	-0.028

Table 6: 2 meter integral value data with comparison

3 Meter

Sphere	Integral Value			Percent Difference Integral Value		
	0-300eV	300eV-2.25keV	2.25keV-10MeV	0-300eV	300eV-2.25keV	2.25keV-10MeV
BSS	1.94E+04	4.54E+03	2.81E+04	---	---	---
3CB	2.02E+04	4.29E+03	2.75E+04	4.186	-5.656	-2.247
3CC	1.84E+04	1.07E+02	3.81E+04	-5.122	-190.815	30.252
3PB	1.84E+04	4.94E+03	3.00E+04	-5.362	8.433	6.653
3PC	1.59E+04	3.64E+03	3.37E+04	-20.099	-21.943	18.328
3WB	1.97E+04	4.92E+03	2.85E+04	1.659	8.061	1.403
3WC	1.83E+04	3.64E+03	3.10E+04	-5.842	-22.099	9.822
5CB	2.03E+04	4.76E+03	2.80E+04	4.574	4.857	-0.412
5CC	2.04E+04	4.58E+03	2.77E+04	4.995	0.825	-1.324
5PB	1.58E+04	3.80E+03	3.43E+04	-20.721	-17.707	19.860
5PC	0.00E+00	0.00E+00	0.00E+00			
5WB	1.85E+04	4.64E+03	2.51E+04	-4.495	2.228	-11.364
5WC	1.80E+04	4.49E+03	2.98E+04	-7.277	-1.103	6.079

Table 7: 3 meter integral value data with comparison

The unfolded $^{241}\text{Am-Be}$ spectra is compared against the International Organization of Standardization (ISO) 8529 standard to validate the spectrum results from the BSS and BSE in this experiment to an internationally accepted standard. The raw detector data for the $^{241}\text{Am-Be}$ is used to determine the calibration factors for air in-

scatter and room-return specific to the detectors used. The air in-scatter comparison in Figure 35 shows that the difference in D_o and σ_r with and without the correction factor is negligible. Comparison of the $^{241}\text{Am-Be}$ data to the ISO 8529 in standard in Figure 36 shows little difference but notice the small shift between the ISO peak and the measured peaks. The format of the ISO 8529 spectra is in a log-log plot, so the $^{241}\text{Am-Be}$ spectra were formatted to match.

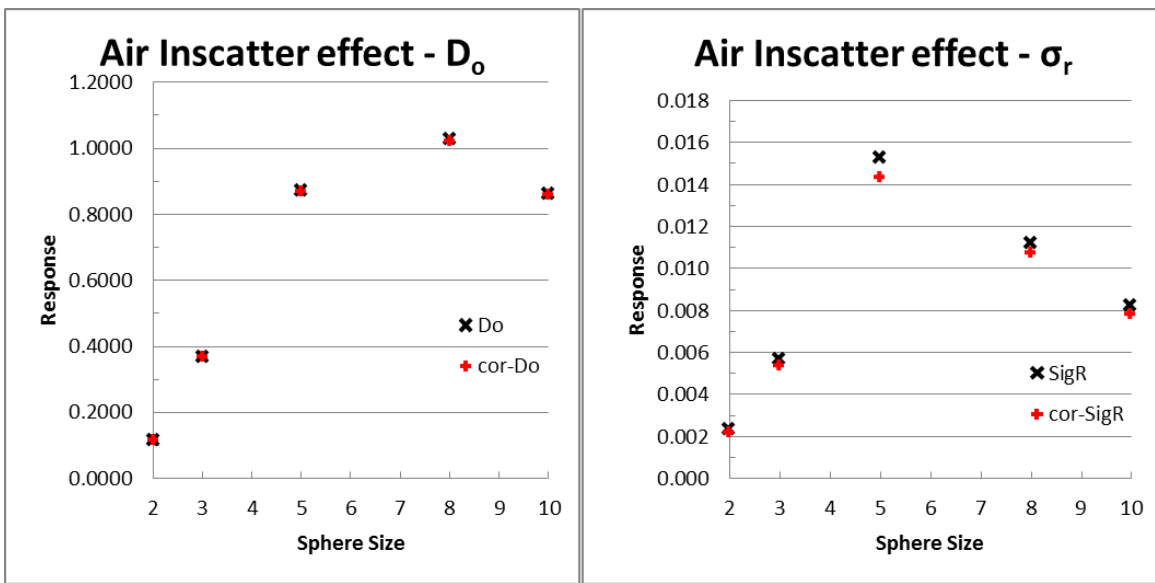


Figure 35: Effect of air in-scatter on D_o and σ_r

Sphere	D_t	With air in-scatter correction		Without air in-scatter correction	
		D_o	$D_t \text{ v } D_o$	D_o	$D_t \text{ v } D_o$
2	0.204372	0.1180	-53.59%	0.1174	-54.06%
3	0.511633	0.3684	-32.55%	0.3693	-32.31%
5	1.0613	0.8684	-19.99%	0.8741	-19.34%
8	1.162943	1.0226	-12.84%	1.0277	-12.35%
10	0.952973	0.8586	-10.42%	0.8632	-9.89%

Table 8: Negligible effect of air in-scatter on total detector response (D_t) and response to source (D_o)

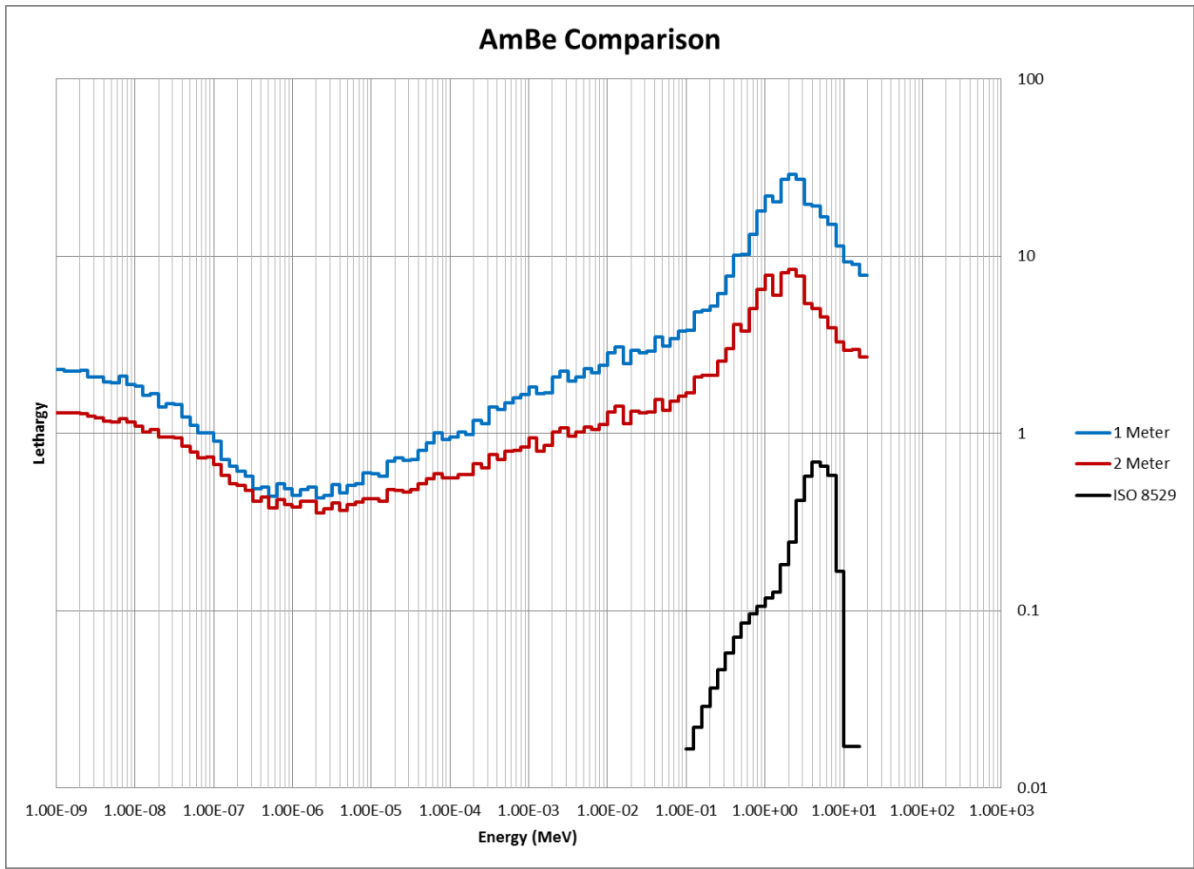


Figure 36: Plot of measured $^{241}\text{Am-Be}$ spectra against ISO 8529 standard

CHAPTER 5: Conclusions

The unfolded neutron spectra appears very similar with most of the peaks appearing in accordance with the Q-value and proton energy. The differences in the spectra can be attributed to the difference in the response functions for the BSE spheres. The BSS spheres which utilize the same response curves have similar shapes and peak locations, with the main difference being the spectra intensities. The varying intensities results from the source to detector distance. As expected from the Q-value of the (n, xn) reaction in the BSE spheres, little information is gained at these low energies. The measured neutron spectrum provides a basic understanding of the shape of the spectrum and the relative fluence rate quantities in thermal, intermediate and fast neutron energies for future experiments using the copper target on the RISE Pelletron. A correlation between this set of Bonner spheres and other well calibrated measurements has been determined using the ^{241}Am -Be measured spectrum allowing for comparisons to other calibration facilities.

Future Work

Response curves that treat the BSE spheres as moderators without an (n,xn) reaction could be calculated using monte-carlo software. The calculated response curves would quantify the efficiency of using BSE spheres at neutron energies below the Q value of the (n, xn) reactions.

A verification of the correction factors calculated from the ^{241}Am -Be is needed. Either an experimental verification with a shadow cone or computational verification using a monte-carlo simulation would be an appropriate verification. The correction values could then be accurately applied to the Pelletron neutron spectrum. After this important verification of the correction factors, a comparison can be drawn between the measurements at RISE and other measurements at calibration facilities for any future neutron detection experiments.

REFERENCES

- Birattari, C. et al. "A Neutron Survey Meter with Sensitivity Extended up to 400 MeV." *Radiation Protection Dosimetry* **44** 1-4, pg 193-197, (2004).
- Bramblett, R.L., Ewing, R.I., Bonner, T.W. "A New Type of Neutron Spectrometer." *Nuclear Instruments and Methods* **9**, pg 1-12 (1960).
- Burgett, E.A. *A Broad Spectrum Neutron Spectrometer Utilizing a High Energy Bonner Sphere Extension*. Thesis, Georgia Institute of Technology. 148 pages, (2008).
- Cruzate, J.A., Carelli, J.L., Gregori, B.N. "Bonner Sphere Spectrometer." Workshop on Uncertainty in Computational Dosimetry: a Comparison of Approaches, Bologna, Italy, pg 44-52, (2007).
- Freitas, B.M., et al. "Scattering Correction for ^{241}Am -Be Calibration of an Individual Albedo Neutron Dosimeter." International Nuclear Atlantic Conference, Recife, Brazil, (2013).
- Glasstone, S., Sesonske, A. **Nuclear Reactor Engineering**, (1967).
- Hsu, H.H., Alvar, K.R., Vasilik, D.G. "A New Bonner Sphere Set for High Energy Neutron Measurements: Monte Carlo Simulation." *IEEE Transactions on Nuclear Science* **41** No. 4, pg 938-940, (1994).
- Hunt, J.B. "The Calibration of Neutron Sensitive Spherical Devices." *Radiation Protection Dosimetry* **8** No. 4, pgs 239-251, (1984).
- International Atomic Energy Agency (IAEA). "Compendium of Neutron Spectra and Detector Responses for Radiation Protection Purposes." Technical Report Series No. 403, (2001).
- International Organization of Standardization (ISO). "Reference Neutron Radiations—Part 2: Calibration fundamentals of radiation protection devices related to the basic quantities characterizing the radiation field, ISO 8529-2." (2000).
- Johnson, T.L., Lee, Y., Lowry, K.A., Gorbics, S. G. "Recent Advances in Bonner Sphere Neutron Spectrometry." Proceedings Theory and Practices in Radiation Protection and Shielding Symposium, Knoxville, TN, pg 83-92, (1987).
- Khabaz, R., Hakimabad, H.M. "Determination of ^{241}Am -Be Spectra using Bonner Sphere Spectrometer by Applying Shadow Cone Technique in Calibration." *Journal of Applied Sciences* **11** (15), pgs 2849-2854, (2011).
- Knoll, Glenn, **Radiation Detection and Measurement**, Third ed. (2000).

- Ludlum Instruments. *Ludlum Model 42-5 Neutron Ball Cart: Instruction Manual*. Sweetwater, TX: Author, 2015.
- McMaster Carr. "Multipurpose 110 Copper." 8966K83 datasheet, (2016).
- National Electrostatics Corp. *12SDH-4 Pelletron: Instruction Manual*. Middleton, WI: Author, 2005.
- ORTEC. *Model 572A Spectroscopy Amplifier: Operating and Service Manual*. Oak Ridge, TN: Author.
- ORTEC. *Preamplifier Introduction*. Oak Ridge, TN: Author.
- Reginatto, M. "The 'few-channel' unfolding programs in the UMG package MXD_FC33, GRV_FC33 and IQU_FC33 for UMG Package 3.3 released March 1, 2004."
- Reginatto, M., Goldhagen, P. "MAXED, A Computer Code for the Deconvolution of Multisphere Neutron Spectrometer Data Using the Maximum Entropy Method." **USDOE report EML-595**, 38 pages, (1998).
- Reginatto, M., Goldhagen, P., Neumann, S. "Spectrum Unfolding, Sensitivity Analysis and Propagation of Uncertainties with the Maximum Entropy Deconvolution Code MAXED." *Nuclear Instruments and Methods A* **476**, pg 242-246, (2002).
- Schwartz, R.B., Eisenhauer, C.M. "Procedures for Calibrating Neutron Personnel Dosimeters." **NBS Publication 633**, 29 pages, (1982).
- Soppera, N., Dupont, E., Bossant, M. *JANIS Book of Proton-Induced Cross-Sections*. OECD NEA Data Bank, pg 238,246, (2012).
- Thomas, D.J., Alevra, A.V. "Bonner Sphere Spectrometers—A Critical Review." *Nuclear Instruments and Methods A* **476**, pg 12-20, (2002).

APPENDIX

Unfolding Output Files

Fluence spectrum from program MXD_FC33				
1	1			
2	39	39	7.37427757923503	0
1.311352599425943E-009	330376795597.595			0.000000000000000E+000
2.331951326809132E-009	154987097994.712			0.000000000000000E+000
4.146861029586860E-009	81212472663.9447			0.000000000000000E+000
7.374277585045714E-009	40528511181.5999			0.000000000000000E+000
1.311352599311132E-008	15495095949.6222			0.000000000000000E+000
2.331951326604965E-008	7027273744.55525			0.000000000000000E+000
4.146861029223795E-008	2303119151.69785			0.000000000000000E+000
7.374277584400083E-008	1157280532.86103			0.000000000000000E+000
1.311352599196320E-007	329944763.287275			0.000000000000000E+000
2.331951326400799E-007	131077427.419136			0.000000000000000E+000
4.146861028860730E-007	75110419.1593537			0.000000000000000E+000
7.374277583754451E-007	45927613.0953365			0.000000000000000E+000
1.311352599081509E-006	24993717.4753085			0.000000000000000E+000
2.331951326196632E-006	18505357.5501603			0.000000000000000E+000
4.146861028497664E-006	13335389.9188442			0.000000000000000E+000
7.374277583108818E-006	10995729.4730314			0.000000000000000E+000
1.311352598966697E-005	10957230.6185967			0.000000000000000E+000
2.331951325992465E-005	6172277.50640107			0.000000000000000E+000
4.146861028134598E-005	6464025.09023467			0.000000000000000E+000
7.374277582463186E-005	4391648.12378779			0.000000000000000E+000
1.311352598851886E-004	2500289.11525268			0.000000000000000E+000
2.331951325788298E-004	2511453.32922485			0.000000000000000E+000
4.146861027771532E-004	2009713.92465851			0.000000000000000E+000
7.374277581817554E-004	1702027.29660061			0.000000000000000E+000
1.311352598737074E-003	900159.590185395			0.000000000000000E+000
2.331951325584131E-003	831285.367674995			0.000000000000000E+000
4.146861027408467E-003	418419.591827587			0.000000000000000E+000
7.374277581171922E-003	324623.693938948			0.000000000000000E+000
1.311352598622263E-002	236146.658288524			0.000000000000000E+000
2.331951325379964E-002	132309.958056953			0.000000000000000E+000
4.146861027045401E-002	68061.1099609198			0.000000000000000E+000
7.374277580526289E-002	60812.2144397138			0.000000000000000E+000
0.131135259850745	37049.3815174863			0.000000000000000E+000
0.233195132517580	27308.6846245303			0.000000000000000E+000
0.414686102668234	12906.8268200940			0.000000000000000E+000
0.737427757988066	6138.81362029899			0.000000000000000E+000
1.31135259839264	393.567662440283			0.000000000000000E+000
2.33195132497163	119.988061305847			0.000000000000000E+000
4.14686102631927	15.4101179139710			0.000000000000000E+000
7.37427757923503	0.000000000000000E+000	0.000000000000000E+000		0.000000000000000E+000

Table 9: Example .flu output from MAXED

```

4m-401
4.6214E+04
  5.0000, 5, 39, 1
    1, 4.7812E+02,1.0680E+02,3.8876E+00
    2,-1.6864E+02,3.2570E+02,1.1856E+01
    3, 1.4099E+02,5.0190E+02,5.1184E+00
    4,-6.6403E+02,2.9020E+02,2.9595E+00
    5, 9.6053E+02,1.4230E+02,1.4512E+00
      -2.6162E-03
1.3114E-09,1.1850E+03,3.3718E+02,3.8841E-03,2.7108E-03,1.2904E-03,3.9202E-04,1.4849E-04,
2.3320E-09,1.1850E+03,2.8129E+02,4.3528E-03,2.8389E-03,1.4302E-03,4.2655E-04,1.5146E-04,
4.1469E-09,1.1850E+03,2.6211E+02,4.5667E-03,3.3759E-03,1.5858E-03,3.9424E-04,1.8566E-04,
7.3743E-09,1.1850E+03,2.3260E+02,5.1057E-03,3.9104E-03,1.8419E-03,4.9369E-04,2.0174E-04,
1.3114E-08,1.1850E+03,1.5814E+02,6.0586E-03,4.2265E-03,2.2485E-03,5.8161E-04,2.3670E-04,
2.3320E-08,1.1850E+03,1.2754E+02,6.8282E-03,5.0236E-03,2.5636E-03,6.7957E-04,2.8875E-04,
4.1469E-08,1.1850E+03,7.4331E+01,8.3186E-03,5.8730E-03,3.0644E-03,7.3868E-04,2.9841E-04,
7.3743E-08,1.1850E+03,6.6419E+01,9.5682E-03,7.6507E-03,3.7797E-03,1.0071E-03,2.7229E-04,
1.3114E-07,1.1850E+03,3.3674E+01,1.1913E-02,1.0195E-02,4.9172E-03,1.2820E-03,4.3893E-04,
2.3320E-07,1.1850E+03,2.3789E+01,1.3176E-02,1.1681E-02,5.8539E-03,1.5173E-03,5.5854E-04,
4.1469E-07,1.1850E+03,2.4241E+01,1.4074E-02,1.3726E-02,6.7010E-03,1.8574E-03,6.5630E-04,
7.3743E-07,1.1850E+03,2.6359E+01,1.3746E-02,1.3933E-02,7.5616E-03,1.9575E-03,7.3536E-04,
1.3114E-06,1.1850E+03,2.5509E+01,1.4116E-02,1.4160E-02,8.0632E-03,2.1930E-03,7.5248E-04,
2.3320E-06,1.1850E+03,3.3586E+01,1.4077E-02,1.5675E-02,9.1524E-03,2.4917E-03,8.6196E-04,
4.1469E-06,1.1850E+03,4.3039E+01,1.3540E-02,1.5609E-02,9.7350E-03,2.8085E-03,1.0160E-03,
7.3743E-06,1.1850E+03,6.3107E+01,1.2664E-02,1.6026E-02,9.9986E-03,2.8571E-03,1.1148E-03,
1.3114E-05,1.1850E+03,1.1183E+02,1.1732E-02,1.6323E-02,1.1133E-02,3.1684E-03,1.0967E-03,
2.3320E-05,1.1850E+03,1.1202E+02,1.1168E-02,1.5588E-02,1.0898E-02,3.1256E-03,1.2291E-03,
4.1469E-05,1.1850E+03,2.0862E+02,1.0037E-02,1.5576E-02,1.1471E-02,3.5789E-03,1.3822E-03,
7.3743E-05,1.1850E+03,2.5205E+02,9.2258E-03,1.5140E-02,1.1882E-02,3.5288E-03,1.3957E-03,
1.3114E-04,1.1850E+03,2.5518E+02,8.8047E-03,1.4110E-02,1.2466E-02,3.7174E-03,1.4595E-03,
2.3320E-04,1.1850E+03,4.5581E+02,7.7026E-03,1.4090E-02,1.2092E-02,3.8985E-03,1.5514E-03,
4.1469E-04,1.1850E+03,6.4862E+02,6.6742E-03,1.3440E-02,1.2666E-02,4.0367E-03,1.5749E-03,
7.3743E-04,1.1850E+03,9.7684E+02,5.9105E-03,1.2944E-02,1.2795E-02,4.4218E-03,1.6885E-03,
1.3114E-03,1.1850E+03,9.1870E+02,5.4930E-03,1.2501E-02,1.3225E-02,4.3306E-03,1.7500E-03,
2.3320E-03,1.1850E+03,1.5087E+03,5.0485E-03,1.2159E-02,1.2448E-02,4.6369E-03,1.6915E-03,
4.1469E-03,1.1850E+03,1.3504E+03,4.6058E-03,1.1147E-02,1.2705E-02,4.6491E-03,1.8123E-03,
7.3743E-03,1.1850E+03,1.8631E+03,3.8384E-03,1.0439E-02,1.2724E-02,4.9722E-03,1.9494E-03,
1.3114E-02,1.1850E+03,2.4101E+03,3.2525E-03,1.0050E-02,1.3319E-02,5.1647E-03,1.9502E-03,
2.3320E-02,1.1850E+03,2.4013E+03,3.2901E-03,9.6955E-03,1.3407E-02,5.3233E-03,1.9786E-03,
4.1469E-02,1.1850E+03,2.1966E+03,2.8119E-03,8.8423E-03,1.3944E-02,5.8364E-03,2.4904E-03,
7.3743E-02,1.1850E+03,3.4902E+03,2.3880E-03,8.4668E-03,1.4167E-02,6.6282E-03,2.7084E-03,
1.3114E-01,1.1850E+03,3.7813E+03,1.8440E-03,7.4555E-03,1.4741E-02,7.7378E-03,3.5029E-03,
2.3320E-01,1.1850E+03,4.9563E+03,1.4236E-03,6.8509E-03,1.5083E-02,9.4984E-03,4.6544E-03,
4.1469E-01,1.1850E+03,4.1656E+03,8.8438E-04,5.1991E-03,1.4525E-02,1.1617E-02,6.5678E-03,
7.3743E-01,1.1850E+03,3.5232E+03,6.9849E-04,3.9054E-03,1.3685E-02,1.4509E-02,9.0256E-03,
1.3114E+00,1.1850E+03,4.0167E+02,4.1287E-04,2.4880E-03,1.0975E-02,1.5272E-02,1.2334E-02,
2.3320E+00,1.1850E+03,2.1777E+02,1.5348E-04,1.4994E-03,8.0212E-03,1.4049E-02,1.2374E-02,
4.1469E+00,1.1850E+03,4.9735E+01,1.7237E-04,9.2460E-04,5.5318E-03,1.1476E-02,1.2197E-02,
7.3743E+00

```

Table 10: Example of .par output from MAXED

Additional Plots of the Neutron Spectrum

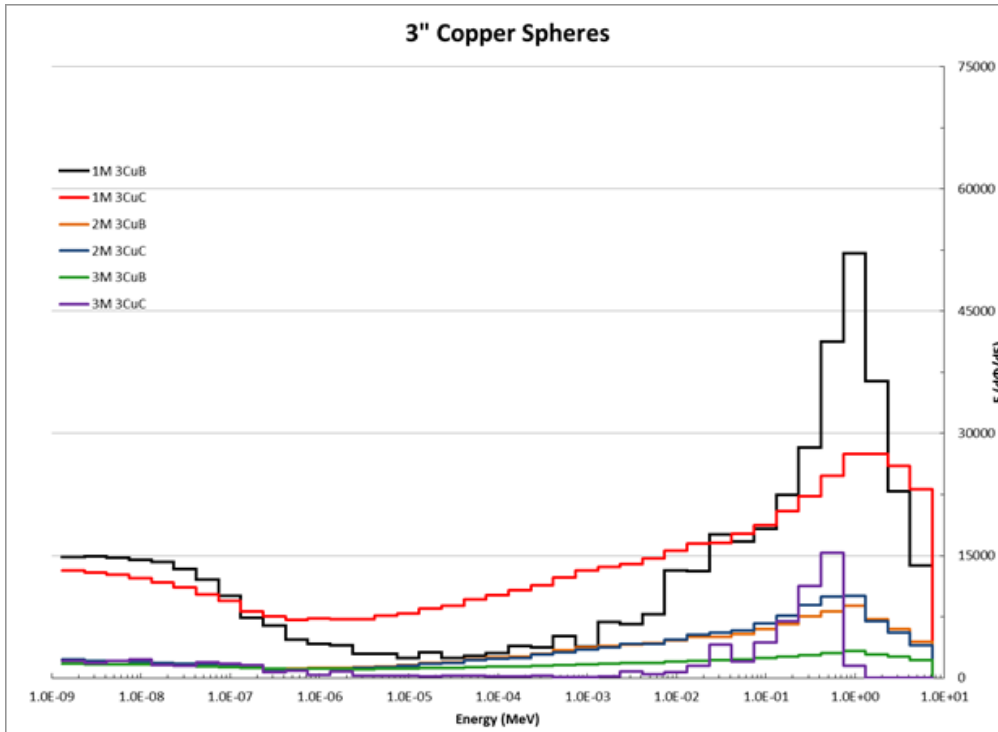


Figure 37: Comparison of 3" copper spheres

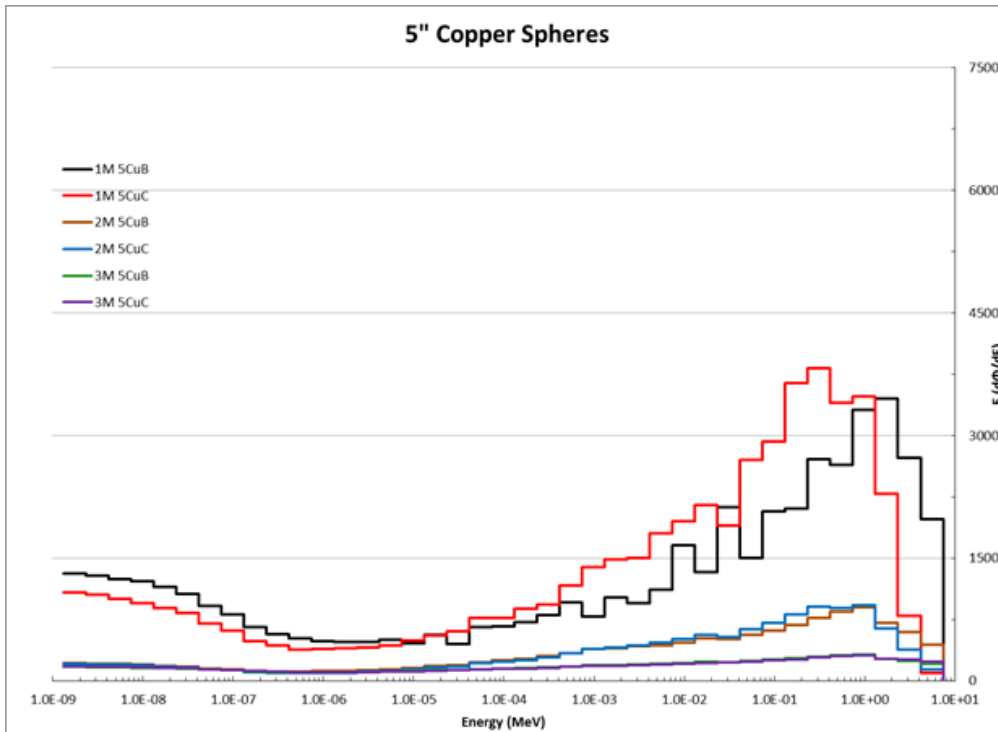


Figure 38: Comparison of 5" copper spheres

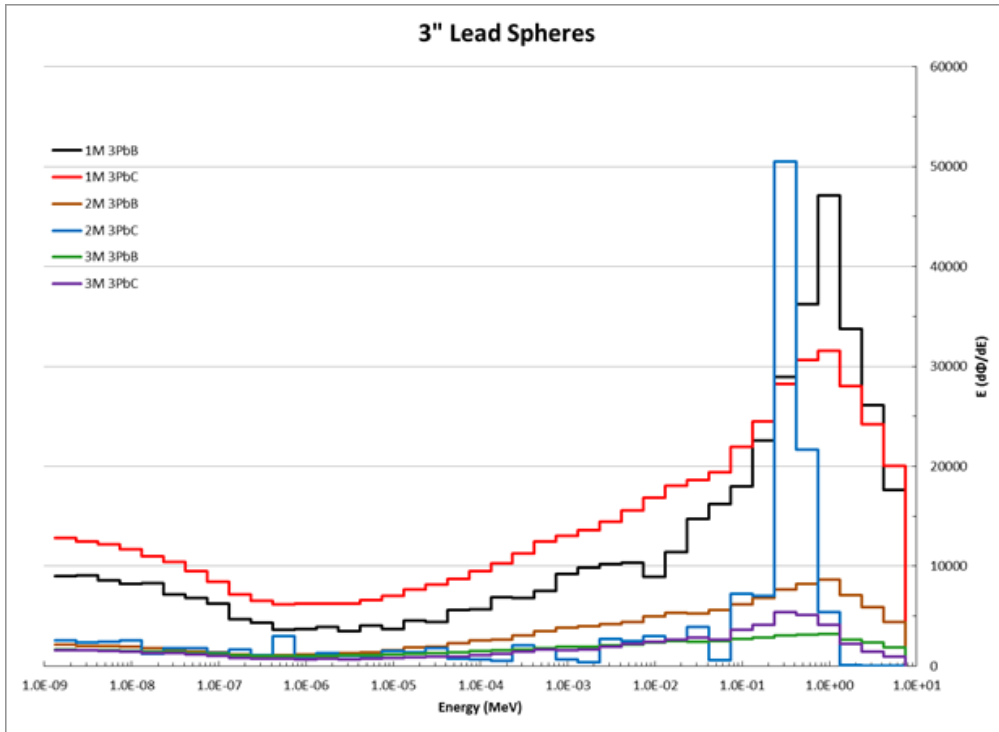


Figure 39: Comparison of 3" lead spheres

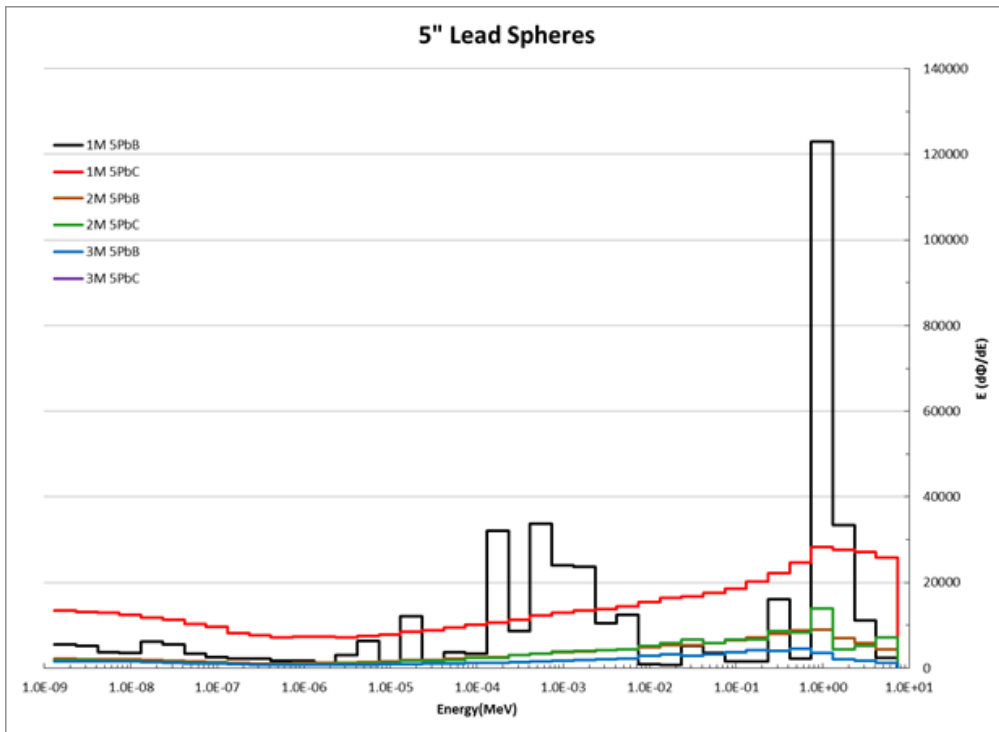


Figure 40: Comparison of 5" lead spheres

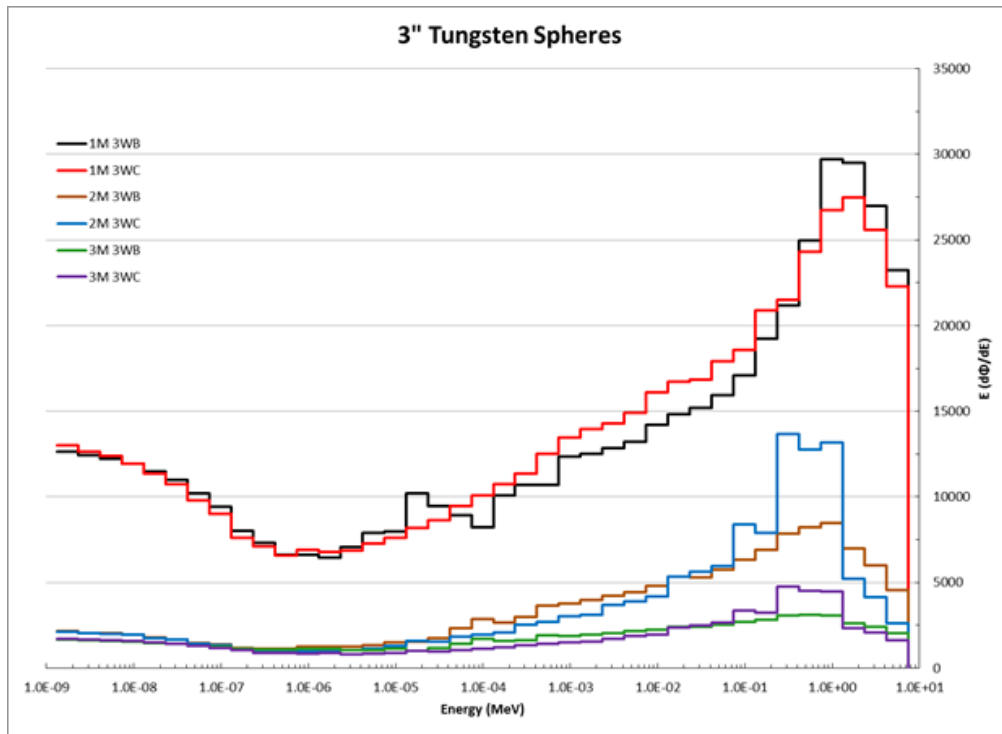


Figure 41: Comparison of 3" tungsten spheres

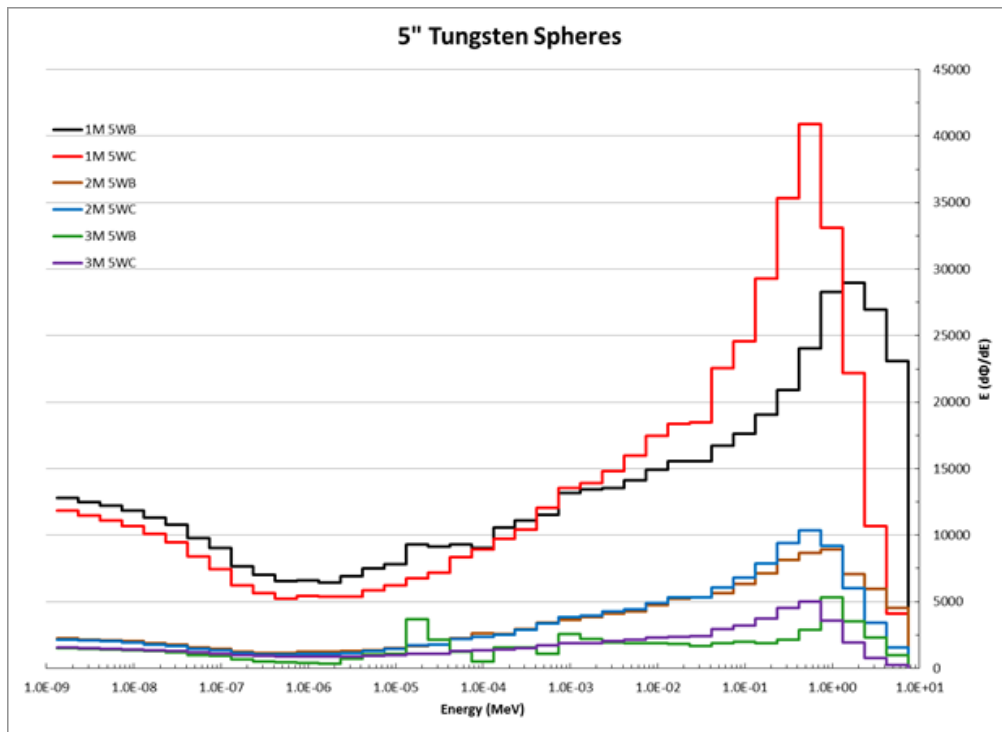


Figure 42: Comparison of 5" tungsten spheres

Percent Difference Plots

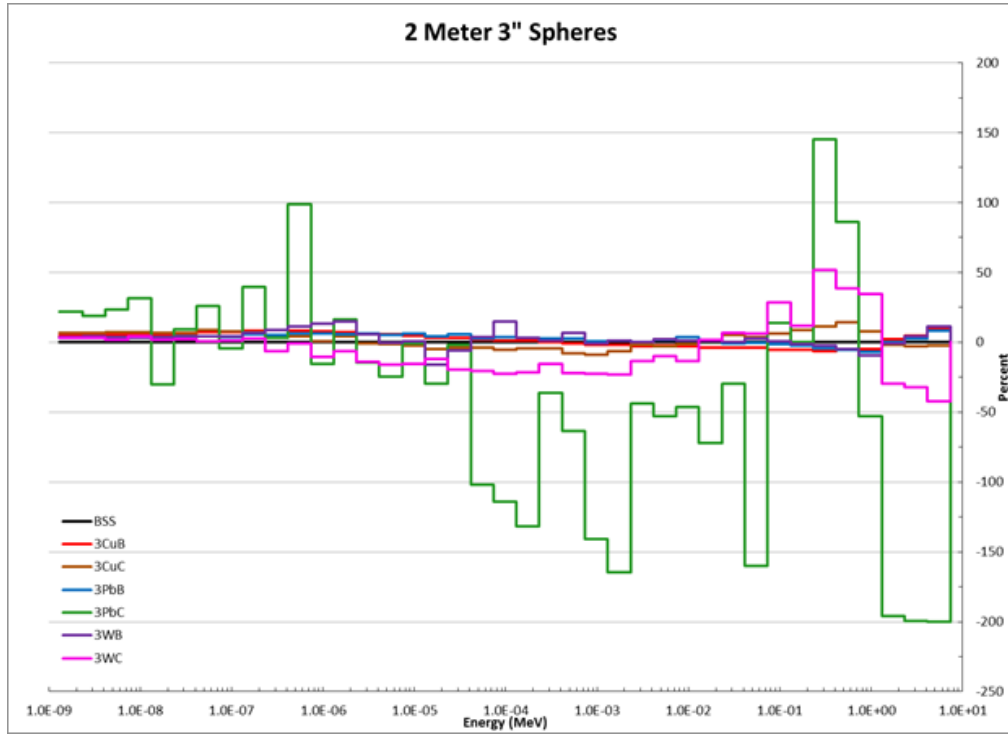


Figure 43: Percent difference in energy bins of 3" spheres at 3 meters

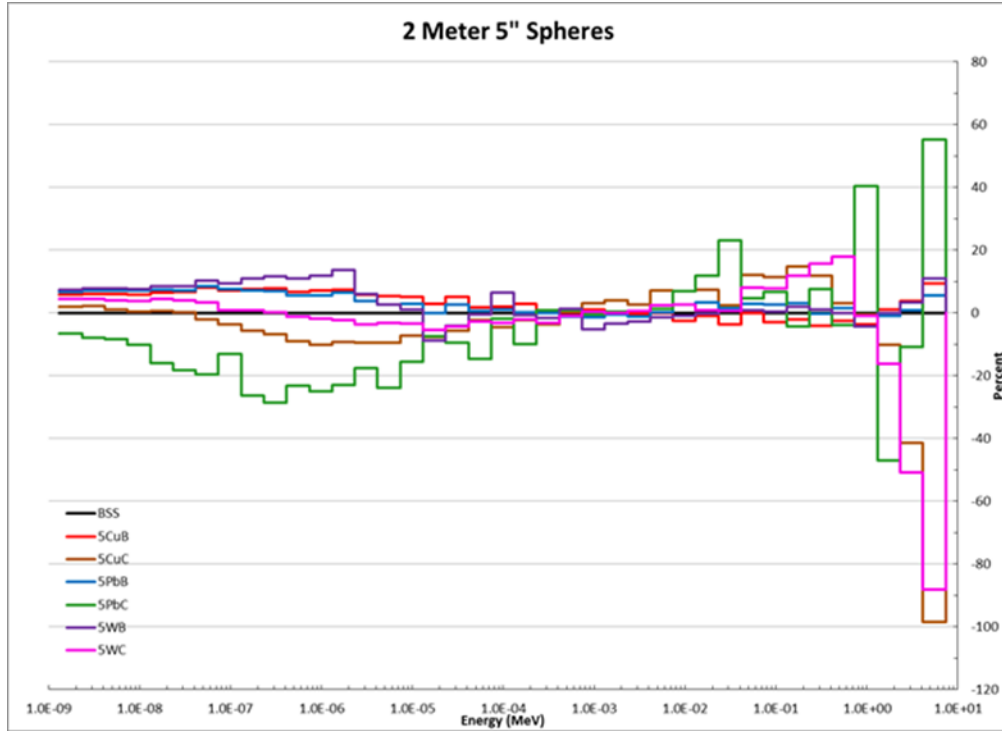


Figure 44: Percent difference in energy bins of 5" spheres at 2 meters

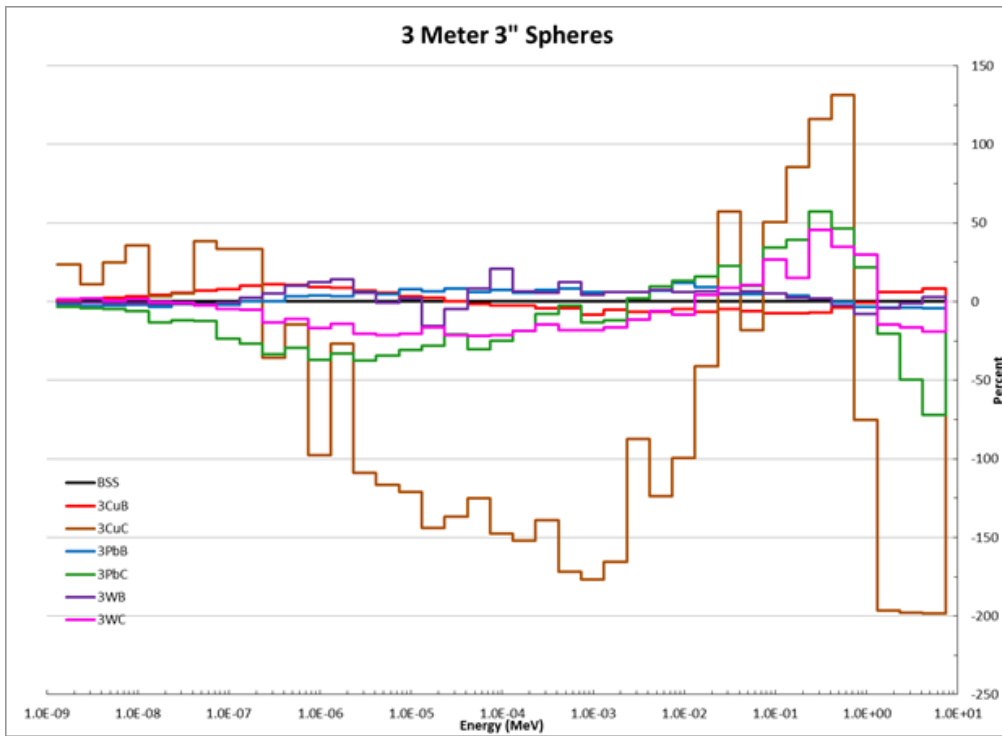


Figure 45: Percent difference in energy bins of 3" spheres at 3 meters

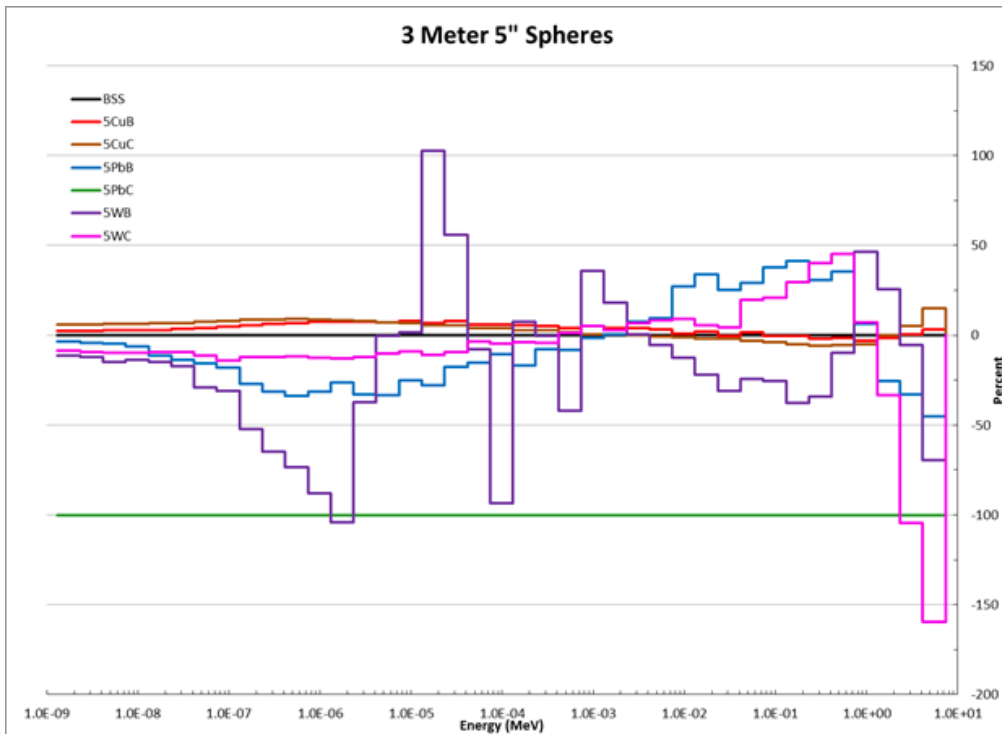


Figure 46: Percent difference in energy bins of 5" spheres at 3 meters

Sphere Properties

Sphere	OD (cm)	ID (cm)	Lip width	Lip Depth	Hole Width	Hole Depth	Assm. Depth	Cyl. Volume
3 Cu Top	12.642	7.643	1.229	0.133				
3 Cu Bottom	12.642	7.643	1.226	0.135	1.981	2.604	9.987	8.102
3 Pb Top	12.662	7.722	1.251	0.157				
3 Pb Bottom	12.664	7.658	1.262	0.152	1.949	2.549	10.556	7.805
3 W Top	12.764	7.811	1.265	0.765				
3 W Bottom	12.709	7.457	1.273	0.749	2.068	2.525	10.132	8.200
5 Cu Top	17.737	12.682	1.151	0.127				
5 Cu Bottom	17.723	12.701	1.346	0.121	1.996	2.604	15.202	8.165
5 Pb Top	17.786	12.865	1.251	0.147				
5 Pb Bottom	17.770	12.833	1.201	0.122	1.981	2.535	15.558	7.889
5 W Top	17.791	12.831	1.222	0.734				
5 W Bottom	17.791	12.672	1.269	0.766	2.045	2.553	15.230	8.199
Lg Cover Top	30.452	17.897						
Lg Cover Bottom	30.471	17.826			5.121	5.817	23.757	46.786
Sm Cover Top	20.300	12.675						
Sm Cover Bottom	20.295	12.715			2.532	3.518	15.621	13.994
2 poly	5.100							
3 poly	7.600							
5 poly	12.700							
8 poly	20.300							
10 poly	25.400							
12 poly	30.500							

Table 11: Physical dimensions of the BSE hemispheres and BSS spheres

Sphere	Weight (kg)	Volume Lg	Volume Sm	Actual		Theoretical	
				Volume	Density	Density	% error
3 Cu Top	3.634	528.90	116.88	412.02	8.82	8.96	1.563
3 Cu Bottom	3.580	528.90	116.88	403.92	8.86	8.96	1.080
3 Pb Top	4.332	531.45	120.53	410.92	10.54	11.34	7.036
3 Pb Bottom	4.274	531.77	117.58	406.39	10.52	11.34	7.257
3 W Top	7.760	544.35	124.74	419.61	18.49	19.25	3.931
3 W Bottom	6.810	537.39	108.58	420.62	16.19	19.25	15.893
5 Cu Top	8.230	1460.82	534.02	926.80	8.88	8.96	0.893
5 Cu Bottom	8.085	1457.37	536.43	912.78	8.86	8.96	1.143
5 Pb Top	9.675	1473.09	557.45	915.64	10.57	11.34	6.822
5 Pb Bottom	9.440	1468.99	553.34	907.77	10.40	11.34	8.297
5 W Top	17.2	1474.35	553.01	921.34	18.67	19.25	3.021
5 W Bottom	15.6	1474.35	532.73	933.42	16.71	19.25	13.181
Lg Cover Top	5.225	7392.97	1500.71	5892.25	0.89	0.935	5.160
Lg Cover Bottom	5.205	7406.85	1482.89	5877.17	0.89	0.935	5.280
Sm Cover Top	1.352	2189.96	533.05	1656.91	0.82	0.935	12.730
Sm Cover Bottom	1.490	2188.32	538.20	1636.12	0.91	0.935	2.600
2 poly	0.060	69.46		69.46	0.86	0.95	9.068
3 poly	0.212	229.85		229.85	0.92	0.95	2.910
5 poly	1.012	1072.53		1072.53	0.94	0.95	0.678
8 poly	4.150	4380.13		4380.13	0.95	0.95	0.267
10 poly	8.090	8580.25		8580.25	0.94	0.95	0.751
12 poly	14.0	14855.87		14855.87	0.94	0.95	0.801

Table 12: Calculated densities of spheres with percent error

Detector Measurement Data

1 Meter Measurement									
Notes									
HV 556-02	+540V						O-Scope	2-4V peak	
Amp 572-02	Gain: 6.9	Coarse: 100	Shaping: 0.5						
Cu - Detector (m):	1								
Detector - L Wall (m):	0.9								
Detector - R Wall (m):	1.1								
			Detector	Beam		Tank	Beam	Integral Counts	+/-
Sphere & Filenames	Integral Counts	+/-	Live Time (s)	Time (s)	CPS	Energy (MV)	Energy (MV)	per mC	per mC
Bare Detector	10081	395	1,863.66	1,845.54	5.462	1.589	3.178	1.024E+02	4.010E+00
2 Bare	16663	495	589.48	550.01	30.296	1.690	3.380	1.315E+03	3.907E+01
3 bare	11272	466	235.34	198.61	56.754	1.690	3.380	2.487E+03	1.249E+02
5 bare	32868	709	345.48	309.73	106.118	1.690	3.380	4.639E+03	1.001E+02
8 bare	32913	830	568.98	521.07	63.164	1.690	3.380	2.913E+03	7.345E+01
10 bare	14420	533	462.90	411.44	35.048	1.690	3.380	1.580E+03	5.841E+01
12 bare	10704	511	769.92	725.20	14.760	1.690	3.380	6.854E+02	3.272E+01
3 Cu bare	13914	489	190.68	157.54	88.320	1.668	3.336	1.924E+03	6.762E+01
3 Cu Covered	11614	472	186.70	167.88	69.180	1.684	3.368	1.549E+03	6.294E+01
3 Pb bare	10907	457	157.36	112.70	96.779	1.693	3.386	2.118E+03	8.875E+01
3 Pb Covered	13739	521	123.22	100.84	136.246	1.682	3.364	2.946E+03	1.117E+02
3 W bare	12492	456	198.52	154.83	80.682	1.690	3.380	1.900E+03	6.936E+01
3 W Covered	14179	591	392.66	373.87	37.925	1.690	3.380	8.877E+02	3.700E+01
5 Cu bare	11955	464	107.70	85.79	139.352	1.685	3.370	2.874E+03	1.116E+02
5 Cu Covered	10112	476	441.88	418.48	24.164	1.690	3.380	5.499E+02	2.589E+01
5 Pb bare	42361	923	358.74	322.55	131.332	1.657	3.314	2.906E+03	6.331E+01
5 Pb Covered	10685	491	240.36	202.75	52.700	1.692	3.384	1.225E+03	5.631E+01
5 W bare	13847	551	142.32	123.91	111.750	1.692	3.384	2.667E+03	1.061E+02
5 W Covered	10269	469	594.54	574.21	17.884	1.687	3.374	4.092E+02	1.869E+01
35 Cu bare	13635	521	174.98	137.04	99.496	1.642	3.284	2.318E+03	8.856E+01
35 Cu Covered	11880	503	580.36	552.65	21.496	1.670	3.340	4.878E+02	2.065E+01
35 W bare	29983	751	471.38	445.20	67.347	1.700	3.400	1.617E+03	4.051E+01
35 W Covered	19038	620	1,988.90	1,958.36	9.721	1.680	3.360	2.319E+02	7.550E+00
35 Pb bare	11874	527	176.52	133.00	89.278	1.687	3.374	2.051E+03	9.105E+01
35 Pb Covered	10975	495	172.22	139.15	78.872	1.694	3.388	1.874E+03	8.454E+01

Table 13: 1 meter Pelletron detector data

2 Meter Measurement									
Notes									
HV 556-02	+540V					O-Scope	2-4V peak		
Amp 572-02	Gain: 6.9	Coarse: 100	Shaping: 0.5						
Cu - Detector (m):	2								
Detector - L Wall (m):	1.08								
Detector - R Wall (m):	0.92								
			Detector	Beam		Tank	Beam	Integral Counts	+/-
Sphere & Filenames	Integral Counts	+/-	Live Time (s)	Time (s)	CPS	Energy (MV)	Energy (MV)	per mC	per mC
Bare Detector*	14949	480	4039.08	4025.71	3.7134	1.675	3.350	9.638E+01	3.090E+00
2 bare	10357	444	755.34	738.96	14.0156	1.675	3.350	3.967E+02	1.701E+01
3 bare	11320	409	424.74	376.13	30.0960	1.673	3.346	8.881E+02	3.209E+01
5 bare	11450	464	342.00	268.73	42.6078	1.673	3.346	1.216E+03	4.927E+01
8 bare	10862	432	397.42	340.17	31.9311	1.690	3.380	8.593E+02	3.417E+01
10 bare	13098	478	857.04	795.48	16.4655	1.690	3.380	3.796E+02	1.385E+01
12 bare	12005	485	1687.74	1549.9	7.7457	1.700	3.400	1.760E+02	7.110E+00
3Cubare	11427	480	488.74	395.94	28.8604	1.678	3.356	7.518E+02	3.158E+01
3CuCov	11751	467	594.88	556.98	21.0977	1.672	3.344	5.105E+02	2.029E+01
3Pbbare	12222	466	423.30	394.4	30.9888	1.677	3.354	8.406E+02	3.205E+01
3PbCov	10967	484	318.42	278.76	39.3421	1.677	3.354	1.026E+03	4.530E+01
3Wbare	10297	441	460.50	438.51	23.4818	1.677	3.354	6.140E+02	2.630E+01
3WCov	10748	457	1221.14	1123.24	9.5687	1.700	3.400	3.514E+02	1.494E+01
5Cubare	20888	673	615.04	579.27	36.0592	1.677	3.354	1.009E+03	3.251E+01
5CuCov*	9509	503	1652.64	1590.42	5.9789	1.679	3.358	1.620E+02	8.570E+00
5Pbbare	20498	613	535.60	495.99	41.3274	1.676	3.352	1.140E+03	3.410E+01
5PbCov	11154	459	847.48	826.66	13.4929	1.677	3.354	3.692E+02	1.519E+01
5Wbare	12637	509	518.02	499.34	25.3074	1.679	3.358	8.725E+02	3.514E+01
5WCov	10318	514	2750.94	2722.66	3.7897	1.679	3.358	1.130E+02	5.630E+00
35Cubare	12720	528	539.60	487.32	26.1019	1.679	3.358	6.783E+02	2.815E+01
35CuCov	10219	455	1815.06	1796.54	5.6882	1.679	3.358	1.617E+02	7.200E+00
35Pbbare	18668	639	664.32	604.86	30.8633	1.677	3.354	7.723E+02	2.643E+01
35PbCov	14250	545	712.88	667.76	21.3400	1.676	3.352	5.565E+02	2.128E+01
35Wbare*	13781	545	737.00	717.69	19.2019	1.674	3.348	4.730E+02	1.870E+01
35WCov	11088	477	3651.38	3619.94	3.0630	1.677	3.354	8.167E+01	3.510E+00

Table 14: 2 meter Pelletron detector data

3 Meter Measurement									
Notes									
HV 556-02	+540V						O-Scope	2-4V peak	
Amp 572-02	Gain: 6.9	Coarse: 100	Shaping: 0.5						
Cu - Detector (m):	3								
Detector - L Wall (m):	0.99								
Detector - R Wall (m):	0.94								
			Detector	Beam		Tank	Beam	Integral Counts	+/-
Sphere & Filenames	Integral Counts	+/-	Live Time (s)	Time (s)	CPS	Energy (MV)	Energy (MV)	per mC	per mC
Bare Detector	8478	448	5168.06	5141.11	1.6491	1.683	3.366	5.199E+01	2.750E+00
2 bare	10391	502	1802	1775.1	5.8538	1.695	3.39	2.070E+02	1.000E+01
3 bare	10193	542	988.18	942.64	10.8132	1.685	3.37	3.863E+02	2.054E+01
5 bare	12173	576	791.98	755.84	16.1053	1.689	3.378	5.757E+02	2.724E+01
8 bare	11160	482	916.18	824.8	13.5306	1.672	3.344	3.468E+02	1.498E+01
10 bare	13649	563	2021.32	1978.18	6.8998	1.676	3.352	1.710E+02	7.050E+00
12 bare	10110	455	3455.18	3360.17	3.0088	1.676	3.352	8.429E+01	3.790E+00
3Cubare	12434	554	929.1	893.83	13.9109	1.675	3.35	3.689E+02	1.644E+01
3CuCov	10747	432	1304.76	1268.54	8.4719	1.682	3.364	2.922E+02	1.175E+01
3Pbbare	10305	452	659.06	660.17	15.6096	1.683	3.366	4.732E+02	2.076E+01
3PbCov	10115	608	846.82	816	12.3958	1.684	3.368	3.899E+02	2.343E+01
3Wbare	10779	483	1224.18	1196.93	9.0055	1.681	3.362	3.042E+02	1.363E+01
3WCov	9569	456	2148.68	2096.02	4.5653	1.7	3.4	1.399E+02	6.670E+00
5Cubare	10167	516	773.82	711.41	14.2913	1.7	3.4	4.683E+02	2.377E+01
5CuCov	10202	478	3761.98	3629.48	2.8109	1.697	3.394	9.390E+01	4.400E+00
5Pbbare	10881	455	576.9	538.73	20.1975	1.684	3.368	6.272E+02	2.623E+01
5PbCov	10965	461	1731	1710.15	6.4117	1.684	3.368	NO DATA	NO DATA
5Wbare	10310	672	1287.22	1085.05	9.5019	1.683	3.366	3.005E+02	1.959E+01
5WCov	9466	654	6221.3	6169.99	1.5342	1.679	3.358	4.095E+01	2.830E+00
35Cubare	35418	855	2772.3	2741.05	12.9213	1.673	3.346	3.689E+02	8.910E+00
35CuCov	10463	463	3693.32	3651.19	2.8656	1.675	3.35	8.017E+01	3.550E+00
35Pbbare	12446	490	843.56	803.54	15.4890	1.684	3.368	4.863E+02	1.915E+01
35PbCov	10795	436	1090.04	1022.72	10.5552	1.684	3.368	3.280E+02	1.325E+01
35Wbare	13509	570	2088.58	1820.26	7.4215	1.691	3.382	2.555E+02	1.078E+01
35WCov	5890	400	6010.9	5911.64	0.9963	1.69	3.38	3.464E+01	2.350E+00

Table 15: 3 meter Pelletron detector data

4 Meter Measurement									
Notes									
HV 556-02	+540V					O-Scope	2-4V peak		
Amp 572-02	Gain: 6.9	Coarse: 100	Shaping: 0.5						
Cu - Detector (m):	4								
Detector - L Wall (m):	116.5								
Detector - R Wall (m):	107.5								
NOTES									
lots of issue with roi stability and pelletron fluctuations									
ROI was initially off . too low									
relocated roi for inital 5bare									
adjusted gain for a second 5bare run									
DONT move gain in the future.									
			Detector	Beam		Tank	Beam	Integral Counts	+/-
Sphere & Filenames	Integral Counts	+/-	Live Time (s)	Time (s)	CPS	Energy (MV)	Energy (MV)	per mC	per mC
2 bare	7043	535	2521.54	2458.91	2.8643	1.685	3.37	1.068E+02	8.110E+00
3 bare	10406	397	1358.5	1224.81	8.4960	1.689	3.378	3.257E+02	1.243E+01
5 bare	16603	475	803.76	784.45	21.1651	1.684	3.368	5.019E+02	1.436E+01
8 bare	10296	385	950.44	881.08	11.6857	1.683	3.366	2.902E+02	1.085E+01
10 bare	10168	431	1870.5	1848.23	5.5015	1.689	3.378	1.423E+02	6.030E+00
12 bare	9398	507	4571.24	4542.6	2.0689	1.687	3.374	5.906E+01	3.190E+00

Table 16: 4 meter Pelletron detector data

AmBe Source Measurements									
Measurement 1: 1 Meter									
Measurement Info: Bonner Sphere (standard set) using AmBe source to determine sphere to sphere relation and room return									
Folder: Detector Laptop: <i>DI Measurements/AmBe Source/1 Meter/</i>									
Sphere	Integral Counts	+/-	Live Time (s)	CPS					Filename
12bare	11611	463	14755.58	7.869E-01	3.138E-02				12bare.chn
10bare	12608	535	13230.18	9.530E-01	4.044E-02				10bare.chn
8bare	64725	1192	55656.22	1.163E+00	2.142E-02				8bare.chn
5bare	24348	741	22941.68	1.061E+00	3.230E-02				5bare.chn
3bare	11863	498	23186.52	5.116E-01	2.148E-02				3bare.chn
2bare	10750	529	52600.26	2.044E-01	1.006E-02				2bare.chn
BareDetector	10327	483	221454.84	4.663E-02	2.181E-03				baredetector.chn
Measurement 2: 2 Meter									
Measurement Info: Bonner Sphere (standard set) using AmBe source to determine sphere to sphere relation and room return									
Folder: Detector Laptop: <i>DI Measurements/AmBe Source/2 Meter/</i>									
Sphere	Integral Counts	+/-	Live Time (s)	CPS					Filename
12bare	10257	444	42042.04	2.440E-01	1.056E-02				12bare.chn
10bare	11405	527	37320.34	3.056E-01	1.412E-02				10bare.chn
8bare	11850	535	30215.78	3.922E-01	1.771E-02				8bare.chn
5bare	23557	791	58058.91	4.057E-01	1.362E-02				5bare.chn
3bare	20163	703	85931.82	2.346E-01	8.181E-03				3bare.chn
2bare	11048	497	94976.74	1.163E-01	5.233E-03				2bare.chn
BareDetector	Power Failure	Run	Terminated						baredetector.chn

Table 17: ²⁴¹Am-Be detector data